POLITECNICO
MILANO 1863

SCUOLA DI INGEGNERIA INDUSTRIALE
E DELL'INFORMAZIONE

Executive Summary of the Thesis

Study on the traces left in minerals by the passage of secondary UHECRs

Laurea Magistrale in Space Engineering - Ingegneria Spaziale

Author: Anita Capelli

Advisor: Prof. Giovanni Consolati

Co-advisor: Lorenzo Caccianiga, Claudio Galelli

Academic year: 2020-2021

1. Introduction

The work in this elaborate focuses on the investigation of the traces left by the passage of a Ultra High Energy Cosmic Ray (UHECR) in several materials, namely basalt, morenosite and halite.
The research developed here is carried out in collaboration with a research group of Statale University of Milan called Gipeto. Their aim is to prove the existence in the past of a particular neutron star in our Galaxy.
According to Bottom-Down theories, neutron stars are one of the best candidates as cosmic rays' accelerator. Among them, Gipeto group specifically focuses on magnetars.
As a matter of fact, magnetars' magnetic field can reach up to 10^{13}-10^{15} G making this class of stars suitable as particles' accelerator [5].
This type of neutron stars is common to standard Galaxies. Therefore, assuming they are present also in the Milky Way is not too outlandish [3].
The most relevant consequence of the existence of magnetars relatively near to Earth, is that, most likely, also cosmic rays of higher energy arrive to our planet.
Indeed, the further is the source of cosmic rays the lower is the energy of these particles. The presence of even one magnetar in our Galaxy entails that the source is sufficiently close that not only low energy cosmic rays are able to reach the Earth, but also particles of higher energy.
Consequently, to study the existence of magnetars is equal to investigate the traces left by high energy cosmic rays.
Cosmic rays are peculiar particles characterized by very high energy ($>10^{18}$ eV [4]). As these particles reach Earth, they interact with the molecules composing it (oxygen, nitrogen and others). The result is a phenomenon called extensive air shower.
The cosmic rays arriving at the atmosphere boarder are usually referred to as primary particles, while the ones generated in the extensive air shower are commonly denoted as secondary particles.
There are several techniques to unveil the former cascade of particles. Each of these requires specific detectors.
The work developed in this project is based specifically on one of these: paleodetectors.
Paleodetectors are nothing other than the employment of a soil's sample to investigate the passage of a cosmic ray. Indeed, among the sec-

ondary particles produced in the extensive air shower, also muons are present. These particles are able to reach the Earth's surface and to penetrate deep in the crust before the decay [1]. Along their path, muons can interact with the encountered atoms leaving a trace of their passage.
The simulations developed in this project focuses particularly on this last process.
Alongside muons, neutrons are also investigated. Indeed, three simulations' scenarios are initialized.
The first is composed of a layer of basalt overtopped by a layer of seawater to have a more realistic scenario. This focuses on the interaction of a muon at different energies with the basalt.
The second and the third simulate a flux of muons first and neutrons second, respectively in morenosite and in halite.
A concise summary of the environments' geometry is given in table 1.

Environment	(x,y,z) [m]
Ocean	(1000,1000,2000) (1000,1000,3700)
Crust	(1000,1000,1000)
Minerals	(1,1,1)

Table 1: Environments' geometry summary.

These simulations are necessary to understand both what should be sought in a sample extracted from the soil and what is the background noise due to latest particles' passages. This is particularly true for the second and third cases which simulate a direct interaction with the secondary particles cited above.
It is important to understand whether these letter traces can cover the ancient ones or not. As a matter of fact, if the older traces are unrecognisable because of the direct exposition, the samples should be shielded once extracted from the soil.
The traces left by muons and neutrons can be of different types. In this work isotopes and radioactive isotopes arising from the passage of the earlier sub-atomic particles are sought.
In table 2, an overview of the case studies simulated in this project is given. The outcomes of these simulations are reported in the next section.
To proceed, it is worth introducing two of the

Scenario	Particle	Energies [GeV]
Ocean and crust	muon	$1x10^3$, $5x10^4$, $1x10^5$
Morenosite Halite	muon	1, 10, 50
Morenosite Halite	neutron	0.001, 0.1, 1

Table 2: Simulations summary.

simulations' settings. These are the particles entrance and momentum direction.
In the first scenario, a single particle enters each simulation always from a fixed point on the top of the Ocean's surface. In the second and the third, several particles (100 000) arrive in each simulation. Their entrance point is not fixed as in the previous case, but it is taken randomly over an area that is the 10% of the total surface. The momentum direction is always set to (0,0,-1).

2. Results

The simulations are carried out employing GEANT4. This is a tool implemented in C++, particularly suitable for Space particles' simulations.
Along with it, also PYTHON and MATLAB have been exploited: the first one to extrapolate the necessary data from the GEANT4 file, the second to filter, when necessary, and analyse the data extrapolated by PYTHON.
GEANT4 produces a huge amount of data. However, the interest in this work is only on isotopes. Hence, these are extrapolated by PYTHON alongside their energy and production's depth and saved onto another file passed subsequently to MATLAB.
In the first case study, further filtering is needed. Indeed, isotopes are also generated in the seawater by the muon's passage. These elements are not relevant, consequently they must be filtered out.
Once this last step is carried out, the data are ready to be analysed.
First, the isotopes are counted on the basis of their mass. Second, they are catalogued on the basis of their mass and energy.
One example of the results of each of these steps is given in fig. 1 and fig. 2. Only these are reported to not overload the summary.

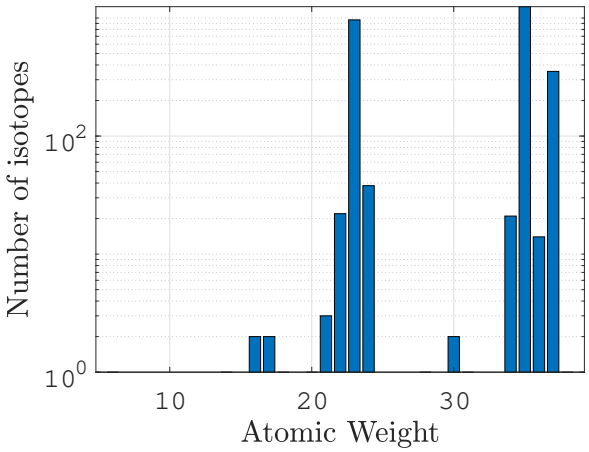

Figure 1: Number of elements produced in halite.

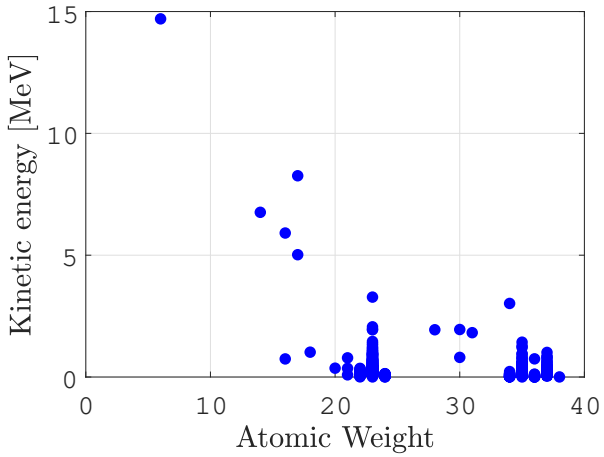

Figure 2: Energy of the elements produced in halite.

To continue with the third and the fourth steps, radioactive isotopes should firstly be found.
Considering as lighter possible element ^{10}Be, the radioactive elements are looked for among the overall isotopes produced. The research is carried out looking at the isotopes' weight.
The choice of ^{10}Be is due to characteristic radioactive elements' half-lives. Indeed, lighter radio isotopes decay much faster than heavier one, precluding the possibility to find them after many years from their production.
Assuming a minimum time interval for the cosmic ray's passage of interest of 100 000 years, ^{10}Be results to be the lighter probable isotope to be still observable after that interval time. table 3 reports all the radioactive isotopes sought in this work.

Isotope $^{A}_{Z}$ element	Half lifetime [y]
$^{10}_{4}$Be	1.5 x 10^6
$^{40}_{19}$K	1.28 x 10^9
$^{144}_{53}$Nd	2.3 x 10^{15}
$^{235}_{92}$U	7.1 x 10^8
$^{238}_{92}$U	4.5 x 10^9

Table 3: Radioactive isotopes with a mean life above 100 000 years from [2].

Unexpectedly, both ^{10}Be and ^{40}K have been found. This discovery allows to follow with the third and the fourth steps.
The first one of the earlier two, computes the fluxes of these two isotopes exploiting the muons and neutrons fluxes measured at sea level.
The equations employed to quantify the fluxes in the minerals are eq. (1) and eq. (2) respectively for muons' passage and neutrons' passage.

$$\frac{d\phi_{isot}}{dE} = \frac{2\pi}{10^5}\frac{d\phi}{dE}N(E) \tag{1}$$

$$\frac{d\phi_{isot}}{dE} = \frac{1}{10^5}\frac{d\phi}{dE}N(E) \tag{2}$$

$\frac{d\phi}{dE}$ is the flux of the muons in the first equation and of the neutrons in the second. These have been retrieved from the experimental ones interpolating the data with MATLAB command `interp1`.
Both the equations are divided by a 10^5 factor because a flux of 100 000 particles has been simulated in the first place.

$$\phi_{isot}(h) = \int_{E_{min}}^{E_{max}} \int_{0}^{\frac{\pi}{2}} N(E)\frac{d\phi_{ocean}(E,\theta)}{dE}s(h,\theta)\,dEd\theta \tag{3}$$

For the first case study, the flux is studied in function of the Ocean's depth. Therefore, before computing it with eq. (3), a sensitivity function has been implemented as in eq. (4). This is the radio isotopes production versus the depth and it has been obtained interpolating the data retrieved with different Ocean's depth through the MATLAB command `fit` to have an exponential. N_0 is the value retrieved from GEANT4 simulations. In eq. (3), the term $\frac{d\phi_{ocean}(E,\theta)}{dE}$ is the flux of muons multiplied by $\cos^2\theta$.

$$s(h,\theta) = N_0 e^{-\frac{\gamma h}{\cos\theta}} \quad (4)$$

An example of the results obtained for the minerals is available in fig. 3 and fig. 4, while fig. 5 reports the isotopes production in the Ocean.

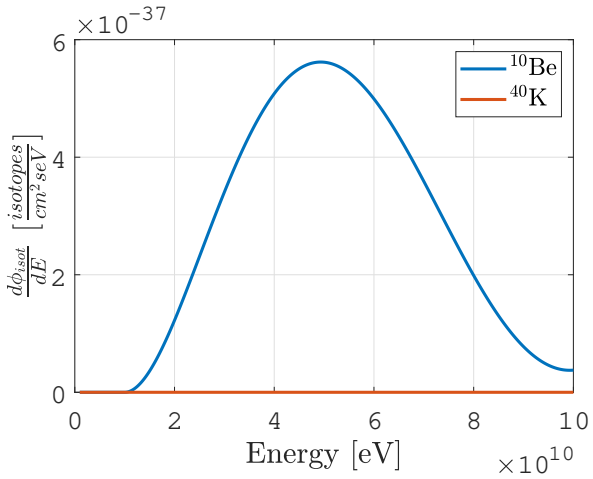

Figure 3: Radioactive isotopes produced by the passage of a $\mu+$ in halite.

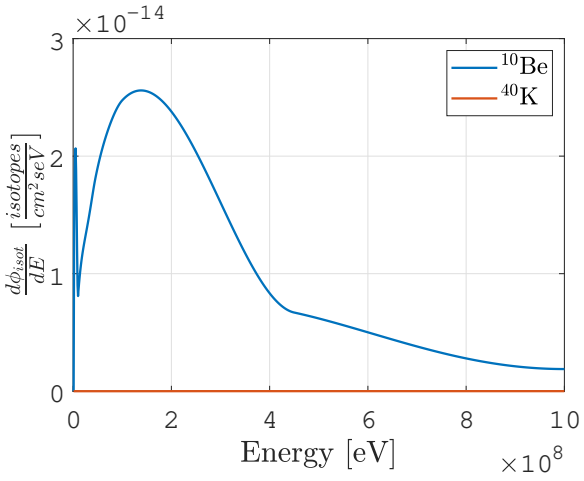

Figure 4: Radioactive isotopes produced by the passage of a n in halite.

The last step studies the propagation in time of the isotopes produced in the three materials to understand the time at which the number of decaying particles balances the one of production. This phenomenon is better known as saturation. Three different situations have been analysed. For completeness, these are reported in table 4. In the previous table, with propagation time is pointed out the overall time of the simulation, while with interval time is addressed the time in between two production's events.

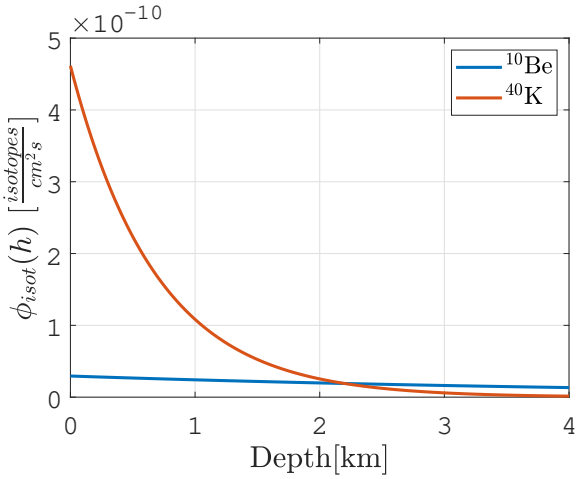

Figure 5: Radioactive isotopes flux produced by the passage of a $\mu+$ in the oceanic crust.

Propagation time	Interval time
100 000	100
100 000 000	1 000
100 000 000	10 000

Table 4: Overview of the propagation's cases analysed.

The case of 100 000 000 propagation years with 100 years between each production is not simulated since it required too much time to run.
From the first analysis none of the radioactive isotopes reaches saturation. Because of this, the other two cases have been arranged.
Nonetheless, since any isotopes saturated, it could be assumed that even lighter than ^{10}Be radio isotopes could be found in that condition. Considering instead 1 000 and 10 000 years the number of radioactive isotopes saturating, increases.
What is interesting to notice is that each isotopes' type almost saturates at the same time regardless of the production time span. An example of this is given in table 5.

Interval time	Saturation time
1 000	31 398 000
10 000	31 400 000

Table 5: Saturation time for ^{10}Be due to the passage of a $\mu+$ of 100 GeV in halite. The propagation time is set to 100 000 000 and different interval time are reported.

3. Conclusions

From the results obtained by the previously mentioned analysis, the use of paleodetectors seems a suitable strategy to study the passage of high energy cosmic rays and, consequently, sources that generate them.
Furthermore, the other techniques to analyse the extensive air shower detect secondary particles such as photons (Fluorescence detector). To identify and study past passage's events, only the employment of a soil sample as a detector can eventually give some results.
Indeed, most of the sub-atomic particles produced in an extensive air shower, can only be directly detected after the passage. The study of traces left by the passage allows to identify and study the past events as the ones that are sought in this project.
The discovery of both isotopes and radioactive isotopes with a sufficiently long half-life leads to believe that exploiting soils samples as paleodetectors to study the ancient passages is the right path to follow.

4. Acknowledgements

I would like to thank professor Consolati for its patience and willingness. Alongside, I need to also thank professor Caccianiga and professor Galelli for following me through all the development of this work. Finally, I want to thank my family and friends to have always supported me throughout my university's career.

References

[1] Richard A. Dunlap. *Particle Physics*. 2053-2571. Morgan & Claypool Publishers, 2018.

[2] Claus Grupen. *Basic nuclear physics*, pages 19–30. Graduate Texts in Physics. Springer, Berlin, Heidelberg, 2010.

[3] Sandro Mereghetti, José A. Pons, and Andrew Melatos. Magnetars: Properties, origin and evolution. *Space Science Reviews*, 191(1-4):315–338, 03 2015.

[4] Manuel Paz Arribas. *Estimation of trigger rates, data rates and data volumes for CTA and observations of SNR RX J0852.04622 with H.E.S.S.* PhD thesis, Humboldt-Universität zu Berlin, 07 2017.

[5] Alessandro Veutro. *Modelizzazione della propagazione di raggi cosmici di altissima energia prodotti da Magnetar galattiche.* Bachelor thesis, Università degli studi di Milano, 2020.

POLITECNICO DI MILANO

Master in Space Engineering

Aerospace Science and Technology Department

Study on the traces left in minerals by the passage of secondary UHECRs

Supervisor: Prof. Giovanni Consolati

Co-supervisor: Dott. Lorenzo Caccianiga

Dott. Claudio Galelli

Thesis by:

Anita Capelli, matricola 939522

Academic Year 2020-2021

"Moi je déclare ne pas en savoir quoi que ce soit.– Mais toujours la vue des étoiles me fait rêver aussi simplement que me donnent à rêver les points noirs représentant sur la carte géographique villes et villages. Pourquoi, me dis je, les points lumineux du firmament nous seraient elles moins accessibles que les points noirs sur la carte de France."

V. Van Gogh, Lettre à Théo

Contents

List of Figures

List of Tables

List of abbreviation and symbols

The following lists are compiled in alphabetical order.

Acronyms and abbreviations

AGN	Active Galactic Nuclei
CMB	Cosmic Microwave Background
EAS	Extensive Air Shower
EHECR	Extreme High Energy Cosmic Ray
GEANT	GEometry ANd Tracking
GRB	Gamma Ray Burst
GZK	Greisen, Zatsepin and Kuzmin
OOA	Object-Oriented Analysis
OOD	Object-Oriented Design
OOT	Object-Oriented Technology
PMT	Photo-Multiplier Tube
TOV	Tolman-Oppenheimer-Volkoff
TTS	Transit Time Spread
UHECR	Ultra High Energy Cosmic Ray
WIMP	Weakly Interactive Massive Particle

Symbols

E	Energy
e -	Electron
e +	Positron
L	Length
N	Number of particles
	Number of isotopes
s(h)	Sensitivity function
γ	Photon
μ	Muon
ν	neutrino
π	Pion
ϕ	Flux

Abstract

The work developed hereafter investigates the traces left by a muon and a neutron in several materials. These particles are commonly found in Extensive Air Shower arising from a cosmic ray passage. Indeed, this work is part of a project called GIPETO which aims to prove the existence of magnetars in our Galaxy exploiting the soil as paleodetector. Two simulation scenarios are arranged to understand the effectiveness of this approach. The first one is composed of one layer of ocean and one of oceanic crust. The second analyses two minerals' samples, one of morenosite and the other of halite. The outcomes are really optimistic. Indeed, among the isotopes produced by the passages, radioactive isotopes with a relatively long half-life are also present. In truth, it is probable to find any of the above in a soil sample nowadays. The results in the minerals can also be seen as background noise. Indeed, direct exposure of the samples to particle showers can cover the ancient traces with newer ones, spoiling the samples used for analysis. Despite this, the use of paleodetectors has shown to be a viable and effective method to identify the historical passing of cosmic rays through different media in the Earth's crust.

Acknowledgments

When it was time to choose my University course, I had a hard time deciding between Aerospace Engineer and Physics. The final choice is clear, but I could not help but being fascinated by everything concerning with Physics. All the intrinsic mechanism and phenomena that stand at the base of our living are just astonishing.

I am grateful to Professor Consolati for giving me the opportunity of combining these two passions in my thesis. I also want to thank him for the patience and interest he has shown towards the project and myself.

I want to thank Professor Caccianiga and Professor Galelli for following me step by step along the development of the thesis. We struggled on GEANT4 and celebrated the found of radioactive elements. Thanks for each correction and suggestion. I really appreciate your patience and your willingness. Even if far apart, I hope you enjoyed the journey as much as I did.

Of course, I cannot avoid mentioning my parents. I have borne in mind the pride on the face of my father the day of my bachelor graduation as well as his persistent questions at dinner time when all I wanted was switching off my mind. They have always been good questions, though, and I will truly never be bored trying to answer you or coupling our knowledge to build the machines of the future whether they are for pine needles or to go on the Moon. Even a huger thanks goes to my mum who has always been present, ready to help me with my university duties and any other difficulty that occurred in my life. I am grateful for all the effort you put in understanding my work and the support you gave me for its realization.

I would also like to thank my granny for whom I have always deserved 30, regardless of the type of exam. She is probably one of my biggest fans and I am glad to make her proud of me.

I need to mention at least other two people that really makes the difference in my life, Teresa and Riccardo. I guess you know the world would be completely different if I did not have you in my life. Probably gloomier. Maybe easier, too. Truly, I think people are not used to say thanks, it is more likely we give people for granted. Well, this is my opportunity to make you feel how important both of you are for me. I have never lived without my little sister and not even ready to stop sharing the room with her. You are a little stubborn crazy ray of sunshine. Instead, it is barely six years that I know you, Riccardo, but at the same time we have been through so much that it is almost like we have known each other for much more time. To both of you goes my heartfelt thanks. I could not ask for better companions.

Certainly, part of the merit of my achievement goes to my friends and colleagues. You have cheered me up each day since we have met. We have shared the good and the bad times. Your support will never be forgotten.

I would like to thank particularly the friends met at the master. I am grateful for having had the opportunity of meeting you and of being able to build a solid and, I am sure, lasting friendship despite the distances due to the Covid pandemic. To those of you who have also been able to come back in Milan to join me in our success, you cannot imagine the joy you brought me today.

Finally, I want to thank myself for never giving up in these years. For the perseverance and the determination demonstrated in the hardest moment. As a good friend of mine would say, not all of us are born Taurus.

Sommario

Il seguente elaborato rientra in un progetto di ricerca chiamato GIPETO guidato da un gruppo di ricercatori dell'università Statale di Milano. Lo scopo di tale progetto è dimostrare che all'interno della nostra galassia vi fossero in passato delle magnetar.
In particolare, questa tipologia di stelle di neutroni è ritenuta un buon candidato come acceleratore di raggi cosmici. Pertanto, la loro esistenza nella via Lattea comporterebbe che particelle ancora molto energetiche, ci riferiamo nello specifico ai cosiddetti Ultra High Energy Cosmic Rays, ovvero particelle caratterizzate da energie oltre i 10^{18} eV, siano state in grado di raggiungere l'atmosfera terrestre e interagire con essa producendo un fenomeno noto come Extensive Air Shower.
Tra le varie particelle secondarie generate si trovano anche muoni e antimuoni sui quali si focalizza l'analisi di questo elaborato. Infatti, queste particelle sono in grado di penetrare anche per diversi chilometri nel terreno lasciando delle tracce nei materiali attraversati.
Questa metodologia di studio dei raggi cosmici viene solitamente indicata come paleodetector.
Di seguito nell'elaborato, congruentemente con la tecnica sopracitata, si ricercano gli isotopi generati dal passaggio di un muone $\mu+$ e di un neutrone n.
In particolare, le simulazioni sono strutturate nel seguente modo:

- Studio del passaggio di un $\mu+$ nella crosta oceanica considerando prima uno strato di oceano. Tre diverse energie sono state simulate in questo caso: 10 TeV, 50 TeV e 100 TeV.

- Studio dell'interazione tra un flusso di 100 000 $\mu+$ e un campione di minerale (morenosite o alite). In particolare, il flusso è stato simulato a tre diverse energie quali 1 GeV, 10 GeV e 100 GeV.

- Studio speculare al precedente con invece di un flusso di muoni uno di neutroni caratterizzati da energie più basse. In particolare, si sono analizzati i casi di 1 MeV, 100 MeV e 1 GeV.

Queste simulazioni sono state svolte con GEANT4, mentre per le analisi sono stati utilizzati in successione PYTHON, per una prima estrapolazione dei risultati dal file GEANT4, e MATLAB per le analisi dei dati filtrati.
In particolare, tramite MATLAB sono stati prima individuati e suddivisi in base al peso atomico e l'energia tutti gli isotopi e successivamente si sono studiati specificatamente quelli radioattivi con peso uguale o superiore a quello del ^{10}Be.

Introduction

When talking about Space, the questions and the issues that the scientific community must face to either understand its physics or explore it are several. Usually, the latter are in synergy and only the collaboration of scientists and technicians allows a true understanding and development of the subject.

For instance, features like cosmic rays need the cooperation of lots of scientific fields, such as physics, engineering as well as geology.

Cosmic rays have been accidentally discovered in the last century. These are characterized by energies spanning from the 10^5 eV to the 10^{20} eV. Yet, no sources or acceleration mechanisms have been established.

However, several possible sources have been identified. Among them, it is worth mentioning the Active Galactic Nuclei and the neutron stars since these are the most accredited ones. The work in this project focuses particularly on the second cathegory of sources.

Indeed, it is developed in collaboration with a research group of the Statale University of Milan, namely GIPETO (Geological Isotopes due to Past cosmic ray Excesses from Transient Objects). Specifically, they aim to prove the existence of a particular type of neutron star in our Galaxy in the past. This class of stars is called magnetar and is characterized by a electromagnetic field sufficiently high to be a reasonable candidate as a cosmic rays accelerator.

This hypothesis has a significant consequence. Indeed, the presence of magnetars in the Milky Way would entail that also Ultra High Energy Cosmic Rays (UHECRs) would have been able to reach the Earth.

Therefore, to demonstrate the passage of these energetic particles would be equal to prove the existence of at least one magnetar nearby.

To accomplish this result, it is essential to define first what to expect from the cosmic rays' passages and second a method to study them.
The cosmic rays interact with the atmosphere when they meet it, producing a shower of secondary particles. This phenomenon is usually called Extensive Air Shower (EAS) and is composed of an electromagnetic and a hadronic part. Both of them can be detected on the ground by exploiting different techniques.
In compliance with the GIPETO project, the focus in this work is on the hadronic cascade. Indeed, this is the part of the EAS composed mainly of muons. These can penetrate deep in the crust leaving a clear trace that can be detected even many years after the actual particle passage.
Lately, a brand-new approach has been established. This is better known as paleodetectors approach. In particular, it provides for the seeking of the traces left by the secondaries produced in the EAS to gain information on the cosmic rays.
The simulations developed in this work, in compliance with the GIPETO project, investigate and analyse the traces left in a few materials.
Specifically, these are the oceanic crust, the and the morenosite. In particular, the first one is over-topped by a layer of seawater for a more realistic scenario.
Considering the latter, three different simulations are arranged. Each simulation investigates at least three different energies per particle. In particular, the first simulation focuses on the passage of a $\mu+$ with 10 TeV, 50 TeV and 100 TeV in the ocean and the oceanic crust, the second investigates a flux of 100 000 $\mu+$ at 1 GeV, 10 GeV and 100 GeV once through halite and then morenosite, the third one is similar to the latter. The only difference is the flux that is composed of neutrons at 1 MeV, 10 MeV and 1 GeV.
All the necessary information for a correct understanding of the simulations are comprehensively discussed in the following chapters. In particular, these are structured in:

- **Chapter 1** - This chapter presents a broad overview of the nature of cosmic rays. It provides a brief description of their composition, followed by an analysis of their spectrum and of their candidate sources. The chapter

particularly focuses on magnetars since these are the ones of interest for the project.

- **Chapter 2** - This chapter is dedicated to the definition of the Extensive Air Shower and the suitable methods to detect it. In addition to this, a section is exploited to sort sub-atomic particles such as muons and neutrons since these are the ones that are produced in the EAS and detected on the Earth's surface.

- **Chapter 3** - This chapter comprehensively describes and justify the choice of the materials for the simulations, namely basalt, halite and morenosite. Moreover, it briefly explains how these materials are implemented.

- **Chapter 4** - This chapter gives a full description of the software used to simulate the passages, namely GEANT4. Furthermore, it presents the code developed specifically for this project and defines the three case studies.

- **Chapter 5** - This chapter collects all the outcomes of the simulations. It also provides an overview of the process exploited to extrapolate the relevant data from the GEANT4 file and to analyse them. For the latter, PYTHON and MATLAB are employed.

Chapter 1

The Cosmic Rays

This chapter gives an overview of the cosmic rays' nature and sources.
The cosmic rays have been accidentally discovered in 1912 by V. Hess thanks to an atmospheric experiment. Actually, the latter was set to study the variation of the Earth's radioactivity at the increase of height. Indeed, at that time, several radioactive isotopes such as U238 had already been found in the terrestrial crust. Consequently, different analysis had been set to characterize what is commonly called Earth's radioactivity.
As already mentioned, Hess was specifically interested in the height variation of the former. To acknowledge it, he decided to exploit an atmospheric balloon provided with all the necessary instrumentation for the measurements.
During the experiment, the researcher observed that after a certain altitude the radioactivity started to increase again. This result was pretty unexpected since the radioactivity was foreseen to continuously decrease going further from the crust.
In parallel, an Italian physicist, Domenico Pacini, also conducted an experiment that led to a similar result.
Both concluded that other particles than the terrestrial ones should exist. These are the cosmic rays.
Cosmic rays are mainly composed of protons, alpha particles and heavier nuclei (98%). On a smaller percentage also electrons and positrons (2%), as well as gamma rays (0.1%), can be found.

Usually, with cosmic rays are identified all the particles coming from sources other than the Earth. These are commonly catalogued based on their energy as it is better explained afterwards in Section 1.1 through a comprehensive description of their spectrum.

Instead, the possible sources of cosmic rays are analysed in Section 1.2. The latter is still an open point for the scientific community. Nonetheless, several hypotheses have been made over the years. The most accredited ones are reported in the previously mentioned section.

1.1 The Spectrum

This section presents the spectrum of the cosmic rays.

The spectrum represents the flux or rather the number of particles per unit of energy, surface, time and solid angle in function of the energy. This is reported in Fig. 1.1.

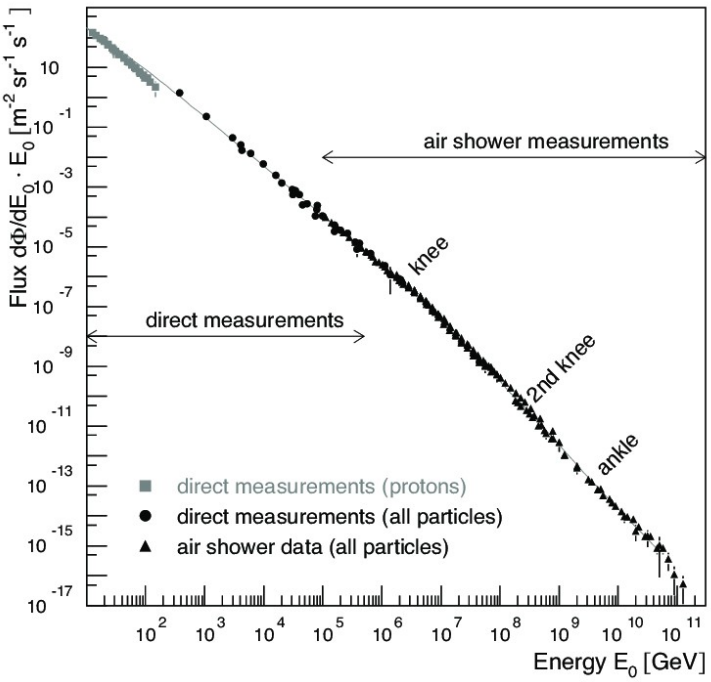

Figure 1.1: Cosmic rays spectrum from [31].

Several features can be pointed out by looking at this figure.
First, depending on the energy, it is possible to identify different types of particles. Two points define the change of variety. These are commonly known as knee and ankle and are found respectively at 10^{15} eV and 10^{18} eV of energy. Studies suggest that each of the previously mentioned points marks the beginning of a new particles' origin. However, the changes are not stark in reality.
Identifying with 1 the portion before the knee, with 2 the portion in between the knee and the ankle and with 3 the remaining portion after the ankle, it is possible to state that:

1. Till 10^{15} eV the cosmic rays belong to our Galaxy. Truthfully, the flux below 10 GeV is observed to be Sun-dependent meaning that the solar activity affects it. This entails that the cosmic rays below that energy arrives not only from our Galaxy but specifically from our Solar System. Above that value, the latter dependence is lost and, henceforth, the flux can be described by means of a power law. Overall, the cosmic rays belonging to this portion are characterized by a high flux, around 1 particle/(m^2s), and are mainly composed of protons (50%), helium (24%), CNO (13%), iron (13%), electrons (1%) and gammas (0.1%).

2. Between 10^{15} eV and 10^{18} eV galactic cosmic rays start to switch to extragalactic cosmic rays. The flux decreases from 1 particle/(m^2year) around the knee to 1 particle/(km^2year) around the ankle. The extragalactic particles are composed mainly of heavy and light atomic nuclei such as protons and alpha particles, as well as by photons and neutrinos [36]. Nonetheless, the latter are believed to be the products of the interaction of even higher energy particles with the surrounding matter.

3. Above 10^{18} eV the cosmic rays are believed to be all of extragalactic origin. The flux reaches down to 1 particle/(km^2century) and less.

As already mentioned, the flux can be described by a power law from 10 GeV on. When transitioning from galactic to extragalactic cosmic rays, the slope of the graph changes. Indeed, the two aforementioned points - the knee and the ankle

- coincide with the changes of the angular coefficient of the graph. The power law is reported in Eq. (1.1) together with the coefficients at the related energies (Eq. (1.2)).

$$\frac{dN}{dE} \propto E^{-\alpha} \tag{1.1}$$

$$\alpha = \begin{cases} 2.7, & \text{E}<10^{16} \text{ eV} \\ 3.1, & 10^{16}<\text{E}<10^{19} \text{ eV} \end{cases} \tag{1.2}$$

To what concerns this project, the focus is on the particles with energy above 10^{18} eV. These are usually denoted as Ultra High Energy Cosmic Rays and are mainly composed of light and heavy nuclei. UHECRs are believed to contain important information about the cosmic accelerators which are discussed in a dedicated section afterwards.

Carrying on with the description of Fig. 1.1, it can be noticed that around 10^{20} eV there is a cut-off. This is better known as Greisen, Zatsepin and Kuzmin (GZK) cut-off and is possibly due to the interactions between the extragalactic cosmic rays and the photons background. Specifically, the interactions occur between the protons and the Cosmic Microwave Background (CMB).

As a matter of fact, the discovery of the CMB has been of particular importance for the definition of the GZK cut-off. Indeed, at very high energies, the Universe is expected to be opaque to certain particles.

For instance, protons can interact with the CMB. The reactions implied are reported in Eq. (1.3).

$$\begin{aligned} \text{p} + \gamma_{CMB} &\rightarrow \text{N} + \pi, & \text{E}_p &\geqslant 1.1 \text{ x } 10^{20} \text{ eV} \\ \text{p} + \gamma_{CMB} &\rightarrow \Delta \rightarrow \text{N} + \pi, & \text{E}_N &\geqslant 2.5 \text{ x } 10^{20} \text{ eV} \end{aligned} \tag{1.3}$$

Each inelastic collision removes a large amount of energy from the particles. As a consequence, it decreases to few EeV after just some Mpc[1]. In Fig. 1.2 the interaction length is described as a function of the energy.

The last feature that can be observed from Fig. 1.1 is related to the methods

[1] 1 pc = 3.26 ly = 3.0857×1016 m

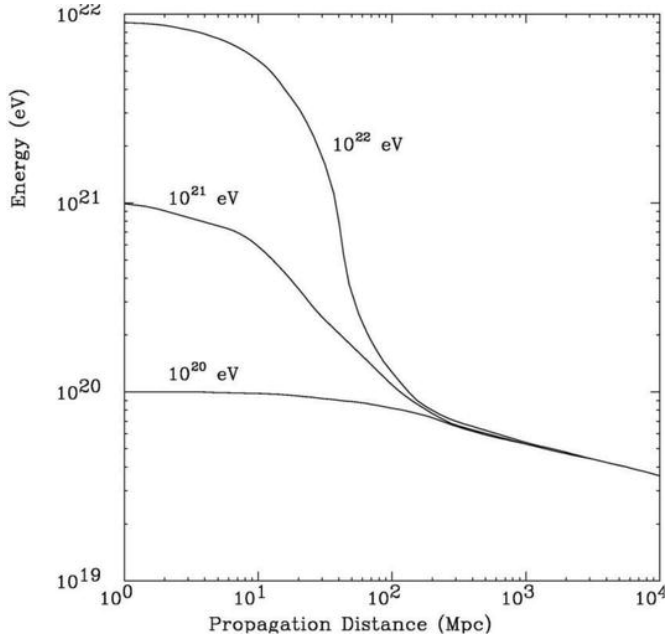

Figure 1.2: Energy degradation for different nucleus energy in function of the distance from [36].

exploited to obtain the experimental data. Indeed, either direct measurements - lower energies - or indirect measurements - higher energies - can be used. The condition for which one is more likely to be used than the other becomes clearer once the fluxes are retrieved. As it has been already said, the higher the energy the lower is the flux. This entails that direct measurements such as those carried out employing balloons are precluded for very high energy particles. Truthfully, the direct detection of the latter would imply using enormous experiments which, obviously, can be sent neither in atmosphere nor in orbit. Given that, UHECRs are the part of cosmic rays of interest for this analysis and the overall GIPETO project. The indirect methods used to detect and study such high energy particles are analysed in chapter 2.

1.2 The Sources

This section analyses all the candidate sources of cosmic rays.

The process through which the particles get accelerated to gain such high energy as well as the source from which cosmic rays are originated are still open questions for the scientific community.

Yet, one of the main issues that needs to be addressed to deepen our knowledge on the matter is related to the particles' nature. As it has been already mentioned, cosmic rays, and particularly UHECRs, are charged particles. Therefore, they interact with the magnetic fields encountered on their path, eventually changing their trajectory. This may still not sound like a core point. Nonetheless, even a slight change in the particle's path towards the Earth furtherly complicates the identification since it entails that the source cannot be sought looking at the incoming particle direction.

Another possibility to acknowledge the source is studying the energy spectrum. Such a process implies the comparison of the experimental data to the modelled ones. The model that resembles the most reality can be considered a good candidate as a cosmic ray source.

Nevertheless, it is still possible to screen a priori some of the ray generator candidates. Indeed, at the heart of this investigation resides the search of an object with a strong magnetic field. Indeed, it is believed that only the latter would be able to confine the particles for the time needed and to accelerate them at the observed cosmic rays' level. Therefore, all the astronomical objects not provided with a strong magnetic field can already be excluded.

Hereafter are presented the sources investigated in recent years. Notice that, two different families have been defined based on the cosmic rays' production process. These are namely Bottom-Up (Section 1.2.1) and Top-Down (Section 1.2.2).

Among the Bottom-Up candidates, one is of main interest for the GIPETO project: the magnetars. For this reason, in Section 1.2.3 this class of stars is extensively described.

1.2.1 Bottom-Up

In this model, a lower energy particle is expected to be accelerated and energized by an astronomical object through electromagnetic interactions. For this reason, the model is called Bottom-Up since it provides for a particle generated at lower energy (bottom) and accelerated to a higher one (up) afterwards.

Fermi has been the first to assume the occurrence of such a mechanism. In 1950,

he proposed the existence of magnetized clouds of gases able to accelerate the particles through electromagnetic interactions. In particular, he supposed that the particles would be bounced back and forth as in a magnetic mirror increasing in each collision their energy. Therefore, considering E_0 the initial energy, the particle would gain

$$\Delta E = \varepsilon E_0 \tag{1.4}$$

per collision thus reaching an energy

$$E_n = E_0(1+\varepsilon)^n \tag{1.5}$$

after n collisions. This process is commonly known as the second order Fermi mechanism. Nevertheless, comparing the results of this model with the experimental ones, some inconsistencies have been observed. Indeed, the spectrum obtained with this model is not congruent with what is experienced. Moreover, the clouds of gases are usually characterized by a poor acceleration efficiency being very slow themselves. Hence, it is unlikely that such objects are able to generate high energy cosmic rays.

Successively, Fermi's model has been revisited (1970). The new hypothesis provides for a shock wave generated by a Supernova explosion. As a matter of fact, the particles crossing the discontinuity would suddenly increase their energy. In particular, the growth would be

$$\Delta E = \beta \frac{3}{4} E_{up} \cos\theta \tag{1.6}$$

where E_{up} is the energy of the upstream particle or rather the one before the crossing, θ is the incidence angle and β is the ratio between the particle and the light velocities[2]. Even if the efficiency is higher than the former Fermi's model, the passage through a shock wave still does not fully justify the presence of cosmic rays of high energy. Indeed, the latter is a fairly rare phenomenon.

Therefore, retaining only the acceleration mechanism, other sources have been

[2] c $\approx$ 3 x 10^8 m/s

sought.

Generally, to understand whether an object can effectively accelerate the particles to the cosmic ray's energy or not, its BR product has to be analysed. In the latter, the B is the magnetic field and the R is the object radius. Indeed, the maximum energy to which the particle is eventually accelerated can be computed with Eq. (1.7) in which Z is the particle charge, B and R are the ones already defined above, and β is the ratio between the particle's velocity and the light one.

$$E_{max} = \beta ZBR \tag{1.7}$$

Furthermore, the Larmor radius of the particles has to be lower than the size of the accelerating object for a certain interval time to energize the particles. As a matter of fact, if the particles escape the object's attraction too early or even immediately, they would not be accelerated whatsoever. Therefore, it is important to take into account both the magnetic field and the radius of the astronomical object concerned.

The former equation can also be studied graphically. Fig. 1.3 reports the Hillas plot or rather the representation of all the astronomical objects that, because of the detection of the right couple of B and R, are suitable as particles accelerators. It is clear that, depending on the particle, different sources should be investigated. These can be retrieved from the former figure. Indeed, the appropriate sources per particle type lie above the line identified by the particle itself.

Looking at the aforementioned figure, it is already possible to grasp that the astronomical objects assumed to be cosmic rays' accelerators are several.

Part of the latter has been listed below with a brief description [37].

- **Active Galactic Nuclei (AGN)** ($\approx$ 1 pc, 10^{-3} G), these are supermassive black holes. Usually, they can be found in the Galaxy's core and are composed of an accretion disk within which the particles are supposed to be accelerated. Indeed, AGN are very energetic astronomical objects. Their magnetic field can reach up to few G[3].

[3] 1 G = 10^{-4} T

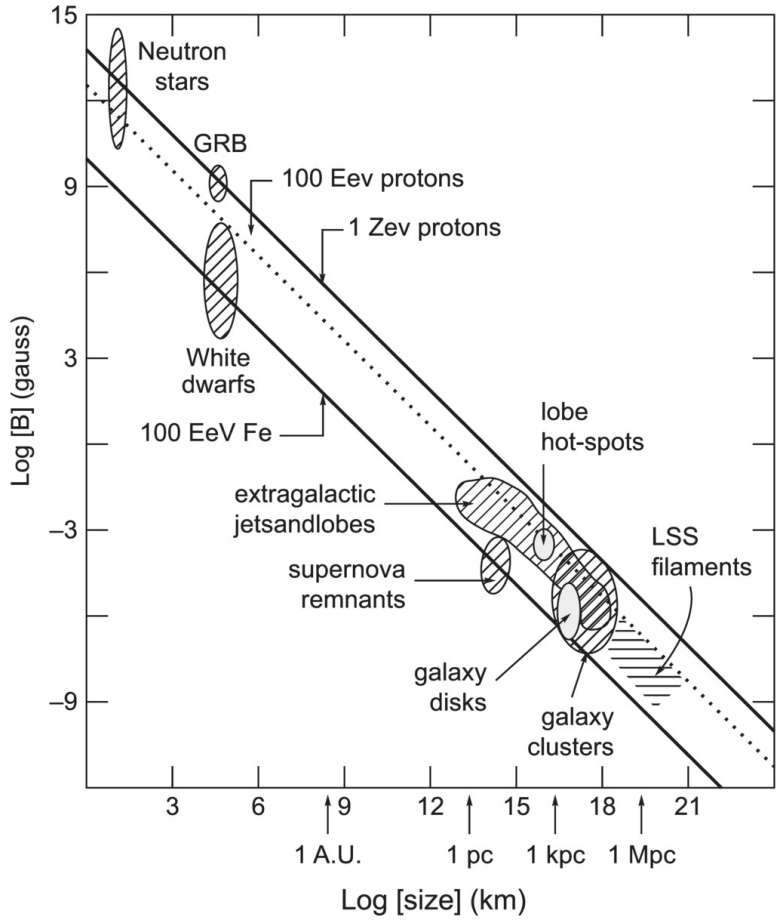

Figure 1.3: Hillas Plot from [20].

- **Galaxy clusters** ($\approx$ 1 kpc, 10^{-6} G), these are able to accelerate theoretically the particles up to 100 EeV thanks to their magnetic field which is of the order of μG. However, within the cluster, the particles can also interact with the CMB. Hence, the expected cosmic rays' energy is limited to a few EeV instead of hundreds.

- **Gamma Ray Bursts (GRBs)** ($\approx 10^5$ km, 10^9 G), these are intense lightnings arising from the collapse of binary systems composed of a supermassive star and a compact object. Theoretically, these bursts would be able to efficiently accelerate electrons and protons. However, since GRBs are cosmological events, their contribution to the cosmic rays' flux is considered to be limited.

- **Neutron stars** ($\approx 10^2$ km, 10^{12} G), these are compact objects usually characterized by very high magnetic fields and angular velocities. The energy of the particles accelerated by these type of stars can be quantified with

$$E_{max} = \frac{\omega}{c} ZBR^2 \tag{1.8}$$

where ω is the angular velocity characteristic of the star and c is the light velocity. B, Z and R are the same introduced earlier while discussing the Hillas plot. A common value for newborn neutron stars is 10^{18} eV of maximum energy. Pulsars and magnetars belong to this class of stars. The seconds, as already mentioned, are the class on which the GIPETO project focuses. The reason for this can be sought in the fact that the latter are provided by the most intense magnetic field among all the neutron stars.

1.2.2 Top-Down

Differently from the Bottom-Up model, the Top-Down one relies on the generation of a particle already with a very high energy which subsequently decays to the cosmic rays' energetic level. The theories belonging to this class are more exotic than the ones of the Bottom-Down model and their description is not strictly required for the sake of this project. However, hereafter a brief introduction of these candidates is also given to have a comprehensive overview of the issue the scientific community is facing.

- **Topological defects**, these are magnetic monopoles or cosmic strings or, more in general, cosmological distributed structures generated right after the Big Bang in correspondence of the intersecting border of two different phases [4].

- **Super-symmetric particles**, these are particles specular to the ones introduced in the Standard model [8].

- **Weakly Interacting Massive Particles (WIMPs)**, the existence of these particles has just been theorized. They are believed to be massive

particles able to interact with the matter through gravity and weak force [30].

1.2.3 Magnetars

Several types of stars exist in our Universe. However, these can be split into three macro-categories on the base of their mass: dwarfs; Sun-like stars; massive stars. The focus here is only on the last class of stars since their remnants can eventually become magnetars.

A star is defined massive whenever it is heavier that $8M_{Sun}$[4]. The process that occur at the end of its life cycle is unique. Indeed, it can turn into either a neutron star or a black hole. Nonetheless, it is worth starting from the beginning to deeply understand the origin of magnetars or more in general of neutron stars. First of all, to study the evolution of stars, two pressures have to be defined: static pressure and degenerate pressure. The first is the classic thermal pressure while the second is due to a quantum effect. In particular, the latter is the pressure applied by the electrons inside the star's body. Subsequently, some reference values have to be introduced to properly understand the evolution of massive stars.

The first landmark is the Chandrasekhar mass. It corresponds to $1.4M_{Sun}$ and quantifies the core mass above which a star collapses and explodes into a Supernova II. As a matter of fact, if the core mass of the star overcomes the Chandrasekhar limit and the nuclear reactions in the star's core are completed, the degenerate pressure is no longer able to withstand the gravitational force. The result is a Supernova II explosion. The process that follows the Supernova explosion is still mostly unknown. However, it has been understood that along with the collapse two main processes occur. These are the photodisintegration of the nuclei into single nucleons, and the reaction between the protons and the electrons. Basically, the consequence of the explosion is that almost all electrons are combined with the protons to form neutrons. Therefore, the remaining core is almost completely composed of the latter.

[4] M_{Sun}=1,989 $\times$ 10^{30} kg

At this point, another reference limit has to be defined. This is the Tolman-Oppenheimer-Volkoff (TOV) mass and corresponds to $3M_{Sun}$. This reference value is fundamental since it discerns stars that evolve in neutron stars from the ones that collapse into black holes. Indeed, the remaining neutrons inside the star's core can apply a degenerate pressure, too. Nonetheless, if the core mass overcomes the former TOV limit, the latter cannot withstand the collapse and the star turns into a black hole.

This work focuses on magnetars which belong to the neutron stars class.

To understand the reason why these stars are suitable candidates as cosmic rays' sources it is important to bear in mind that the angular momentum and the magnetic flux are conserved. This entails that, while the radius decreases due to the collapse, the angular velocity and the magnetic field increase. For instance, the latter can grow up to 2 x 10^9 the initial value. Recalling Eq. (1.8) it is clear that the maximum achievable energy can be huge.

Specifically, magnetars can reach up to 10^{13}-10^{15} G. This qualifies them as good candidates as UHECRs generators.

The hypothesis of this work is that such energetic astronomical objects existed also in the Milky Way. This supposition is not too unrealistic since magnetars have been observed in standard Galaxies and in the Magellan cloud [25]. Truthfully, some have already been identified in our Galaxy too. Nonetheless, these are in concrete less energetic than what is expected on the base of theory. This can be justified considering that all objects in the Universe lose energy over the years, magnetars included. Thus, it can be concluded that, in the past, the same stars observable today might have had enough energy to generate UHECRs.

Proving the presence of isotopes in the terrestrial crust due to the UHECRs passages would also demonstrate the existence in the past of more energetic magnetars. Indeed, the presence of these stars in the Milky Way would entail that UHECRs have eventually reached the Earth leaving traces that should be still detectable nowadays.

The traces that have to be sought are better explained afterwards within chapter 2.

Chapter 2

Cosmic Rays' Detection

In this chapter, the methodologies to detect and study cosmic rays are introduced. The nature of these peculiar particles has been already analysed in chapter 1. However, it is worth recalling at least one of their features before introducing the detectors, namely the spectrum. The examination of Fig. 1.1 clarified that, depending on the energy of the cosmic ray, the flux can either be detected directly, for instance by atmospheric balloons, or indirectly.

UHECRs need to be studied through indirect methodologies since they are characterized by a flux around 1 particle/(km^{2}year).

Basically, the indirect methods rely on the identification of particles generated by the interactions of the UHECRs with the atmosphere. Usually, the resulting particles belong to what is better known as Extensive Air Shower. A comprehensive description of this phenomenon is available in Section 2.1.

Essentially the EAS is a melting pot of secondary particles to which also muons belong. Given that these last particles are more relevant for this work, in Section 2.2 the muon nature is investigated alongside a brief overview of all subatomic particles produced in the EAS. This introductory part is added to have a clear and comprehensive understanding of particles physics.

Finally, the current technologies to detect the EAS are introduced in Section 2.3. In particular, two of them are to be considered brand-new methodologies. Following in the dissertation, these are referred to as modern techniques and regard principally the research of either isotopes or nuclei recoils. However, as presented

in the aforementioned section, they both rely on the same principle which is at the base of this project and justify the development of this work.

2.1 EAS

In this section, the EAS produced by an energetic particle in the atmosphere is discussed. Moreover, its development is determined until it arrives at the ground. In the generation of EAS, the main players are the primary particle and the atmosphere. The latter is composed primarily of nitrogen (78%) and oxygen (21%) with a smaller percentage of argon (0.9%) and other gasses (0.1%) [28]. All these molecules are the ones that the cosmic ray, either a UHECR or other types, meets crossing the atmosphere.

Interacting with the former, the ray, or rather the primary particle, with energy greater than 10^{14} eV, generates a cascade of secondaries, the aforementioned EAS. Specifically, at the first encounter with the atmosphere, pions π are usually produced [36]. These can be either neutral or charged.

The first are around the 33% of the overall number generated in each collision and decay after a short time interval[1] giving rise to a couple of photons γ. These in turn interact again with the air producing a couple of electron e- and positron e+. If the e- path gets deflected, the electrons radiate other photons due to the bremsstrahlung effect. Indeed, as a consequence of the deflection, the electrons lose energy radiating a γ. At this stage, the process starts again with the generation of a couple of e- and e+ and again of γ. The latter is better known as electromagnetic cascade.

The particles produced along the shower can be evaluated with Eq. (2.1)

$$N(x) = 2^{\frac{x}{L_0}} \tag{2.1}$$

where L_0 is the length after which a photon is emitted. The cascade stops once the critical energy E_c is reached.

[1] π^0 mean lifetime = 8.5×10^{-17} s, $\pi^{\pm} = 2.6 \times 10^{-8}$ s.

Considering

$$N_{max} = \frac{E}{E_c} \tag{2.2}$$

$$x_{max} = \frac{L_0}{\ln 2} \ln \frac{E}{E_c} \tag{2.3}$$

and knowing the energy of the incident cosmic ray E and the critical one E_c, it is possible to compute the maximum value of secondary particles produced and the height at which this value is achieved. Once these parameters are acknowledged, the electromagnetic shower development can be studied in its completeness.

Notice that, the critical energy depends only on the atmosphere. Therefore, to quantify it, it is sufficient to compute N_{max} and x_{max} at the time of the cosmic rays' passage.

Differently from the just presented neutral pions, the charged ones are characterized by a longer lifetime. Particularly, the π- can eventually interact with the atmospheric nuclei giving rise to a new generation of neutral and charged pions that sum up to the previous ones. Instead, the $\pi+$ decay into a muon μ and a muon neutrino ν_μ. Ultimately, all the charged pions turn into one of the just mentioned secondary particles and the cascade, better known as hadronic cascade, stops.

The two cascades take place simultaneously each time a cosmic rays arrives into the atmosphere. However, depending on the primary type, one of these can be more developed than the other. By this is meant that the heavier is the cosmic rays, the larger is the probability to have a more significant hadronic shower rather than an electromagnetic one [36] and vice-versa.

Either way, the EAS evolves mainly in two directions: longitudinally and transversely. These are exploited individually or coupled for the identification and study of the EAS. A full explanation of these detecting processes is given in Section 2.3.

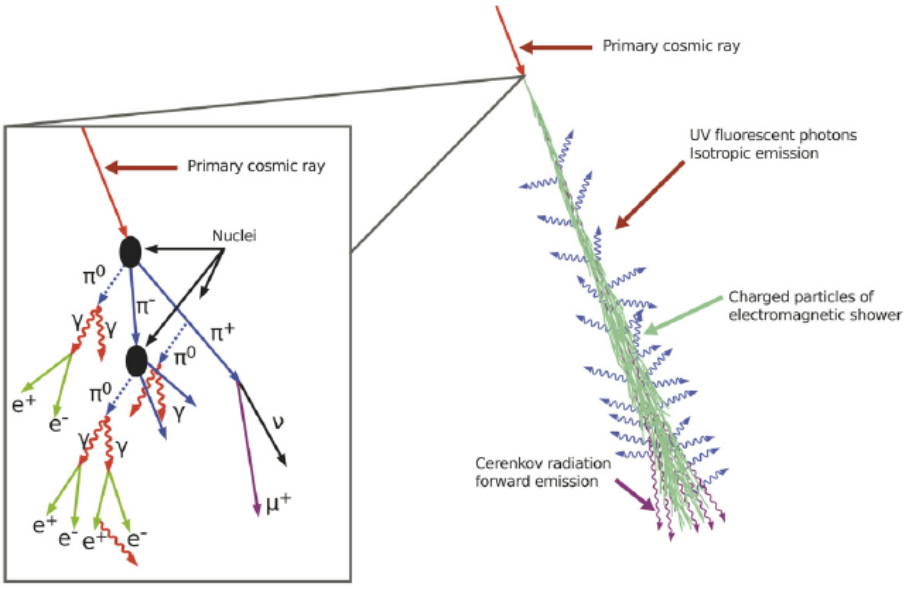

Figure 2.1: EAS development - hadronic and electromagnetic shower from [3].

2.2 Secondary Particles - Muons

In this section, the sub-atomic particles and particularly the muons are concisely introduced.

Commonly, sub-atomic particles are subdivided into two main categories [10].

On one side there are the elementary ones. These are at the basis of all the matter. They can be split again into fermions and bosons based on their spin [10]. Among the fermions, it is possible to find quarks, leptons and their counterparts. All of them are also known as matter and anti-matter particles. As reported afterwards, μ belongs to the leptons' class.

On the other side, there are the composite sub-atomic particles. A special class of them is hadrons, to which all the particles composed of only a few elementary particles belong [10]. Again, these can be subdivided between baryons and mesons. The firsts are usually composed of an odd number of quarks. The seconds, instead, are composed of quarks and anti-quarks. Neutrons are a type of baryons, while pions π belongs to the mesons.

In Fig. 2.2 the aforementioned classes and particles are sketched.

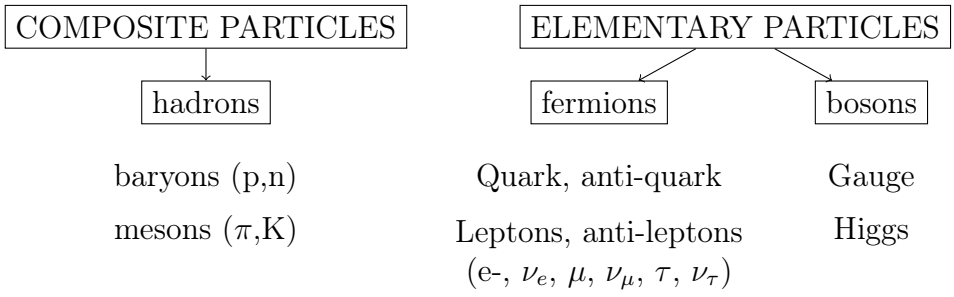

Figure 2.2: Sub-atomic particles.

As a matter of fact, several of them have been cited in Section 2.1 as a result of the interaction between the UHECR and the atmosphere. Truthfully, the former explanation greatly simplifies the process. In reality, all these particles can be produced along with the EAS development.

Nonetheless, this work focuses mainly on one of them, the muons.

As mentioned earlier, these belong to leptons together with electrons, electron neutrinos, muon neutrinos, taus and tau neutrinos. Indeed, this class of sub-atomic particles is composed of both charged (e, μ, τ) and neutral (all neutrinos) particles which are created in couples at each interaction.

What differentiates an electron from a muon and a tauon is the mass and the mean life. An overview of the latter is given in Table 2.1.

Table 2.1: Leptons mean time and mass from [18].

Particle	**Mean life [s]**	**Mass [GeV/c^2]**
electron	stable	5.110 x 10^{-4}
muon	2.19 x 10^{-6}	0.105
tauon	2.90 x 10^{-13}	1.777

Excluding stable particles such as electrons, muons are one of the longest living particles. In addition to this, the ones produced along the EAS are provided by very high velocities. This entails that, for relativistic reasons, time passes more slowly for them and thus they can reach the terrestrial surface before their decay. The interactions between the matter and the muons are similar to the ones between the matter and the electrons. Indeed, the former can be considered as more massive electrons. However, precisely the fact that their mass is far greater than

the one of the electrons ensures that the deceleration they undergo, due to the electromagnetic field, is lower. Consequently, also the bremsstrahlung radiations are of lower intensity. Therefore, the particles arrive on the surface with higher energy and extend deeper into the soil.
For the latter features - the mean lifetime and the ability to penetrate in the soil - the muons are the proper particles to be sought.
In addition, there is another feature that makes these particles really suitable for the study of EAS and cosmic rays. This is their capability of interacting with nuclei in the crust leaving traces of their passage. Searching for the traces, it is possible to reconstruct the muon's energy and demonstrate the cosmic ray's passage.
The μ- are even able to substitute an electron in an atom. Obviously, the atom gets deformed by the muon being far heavier than the electron. However, the formation of such an atom, namely a muonic atom, is a really rare event. Hence they are never sought to study cosmic ray's passages.

2.3 The Detectors

In this section, the practical methodologies for EAS detection are investigated.
It has been already extensively dealt with the problem at the base of cosmic ray's detection and the need to use indirect methodologies. It should be clear at this stage that the detection of the EAS is the only possibility to unveil the presence of a high energy cosmic ray.
To observe and study the EAS, several type of detectors can be exploited. Each of them relies on a particular phenomenon related to the EAS' development.
The main methodologies used for the EAS' detection are reported in Fig. 2.3.
For the sake of clarity, it has been decided to subdivide the techniques used for the detection into two classes. These are:

- Classical techniques, the ones that provide for the observation of the secondary particles either in the atmosphere or on the surface as soon as the particles reach it.

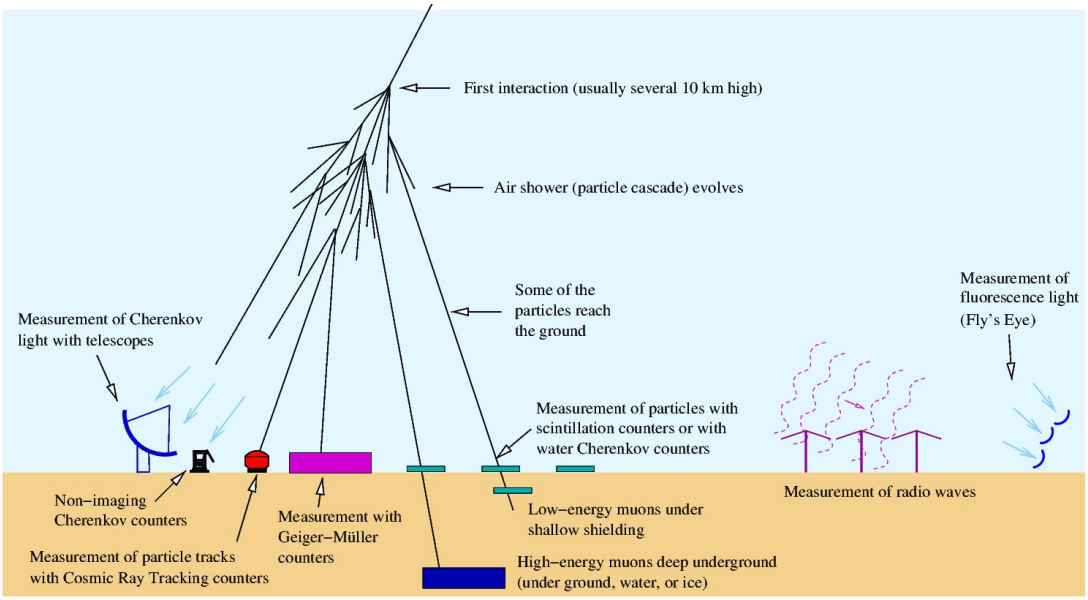

Figure 2.3: EAS detectors from [19].

- Modern techniques, the ones that search for the traces left by a secondary in the soil.

The first ones rely more on the detection of the electromagnetic and hadronic showers, while the second ones are based principally on the identification of the traces generated by the hadronic cascade in the crust. Moreover, some differences are present even among the methodologies belonging to the same class.
The full explanation of all classes of detection's technique is available in Section 2.3.1 and Section 2.3.2, respectively divided for classical and modern techniques.
Notice that the modern ones had to be necessarily introduced since they are at the basis of the functioning of paleodetectors and the development of this work.

2.3.1 Classical Techniques

In Section 2.1, describing the development of the EAS, two directions have been identified. Specifically, these are the transverse and longitude ones.
As a matter of fact, the telescopes belonging to this first class of detectors rely on the analysis of either one of these two or even both.
In particular, the detectors exploiting only one direction at the time are either

ground arrays that sample the particles at the ground and consequently study the transverse development of the EAS, or fluorescence detectors which analyse, instead, the longitudinal development of the shower.
These two instrumentations are described hereafter starting from the definition of the ground arrays. For each method, examples of real infrastructures are also provided.
As mentioned few lines above, these two detection types of equipment can be exploited also synergistically as it is done in telescopes such as the Auger or the Telescope Array. Afterwards, these are also briefly described.

Ground arrays telescope. These are a grid of detectors covering a well-defined area. Usually, the detectors are spaced with distances that range from 100 m to km and are widespread over several km^2.
The spacing is usually related to the typical transverse extension of an EAS produced by a UHECR. For a similar reason, these telescopes are commonly built between 1000 m and 1500 m above sea level. This choice is not accidental but coincides with the height at which an EAS generated by a UHECR reaches its maximum production of secondaries. Hence, these value corresponds to the x_{max} parameter, defined in Section 2.1.
A sketch of a ground arrays telescope is reported in Fig. 2.4 [9].

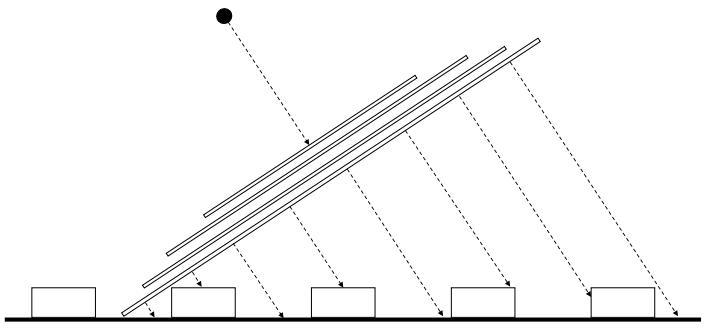

Figure 2.4: Ground arrays telescope.

The instruments commonly used to build such a telescope are plastic scintillators and Cerenkov detectors. These are drawn as boxes in the former figure.
Two are the main features that give information about the primary, namely:

- The density distribution from which it is possible to understand the impact point of the shower.
- The arrival time to understand the shower impact angle at the ground level.

For the second, the Cerenkov detectors result to be a better choice since they can more accurately measure the arrival time.
Finally, it is also possible to count the arriving particles and study their nature.
The first telescope exploiting this technique was Agasa.
It was located in Japan and worked till roughly 2003. It was composed of 111 detectors equally spaced with 1 km of distance between each other, covering an area of about 100 km^2. In particular, it was provided with scintillators to identify electrons, 27 muon detectors and 1 plastic scintillator with several proportional counters [9].

Fluorescence detectors. It is fundamental to bear in mind that the atmosphere acts as a huge scintillator when crossed by a charged particle.
This is due to the presence of nitrogen. This element is excited by the UHECR's passage. During the de-exciting process, it produces a photon at a wavelength of 300 - 400 nm. This corresponds to the UV range which is a part of the light spectrum to which the atmosphere is transparent. Therefore, the photons are able to reach the ground where an array of Photo-Multiplier Tubes (PMT) registers their passage [9]. An example of this infrastructure is given in Fig. 2.5.
Through this technology, it is possible to gain information about several features:

- The number of γ versus time that allows determining the development of the electromagnetic shower.
- The direction and nature of the impacting cosmic ray.

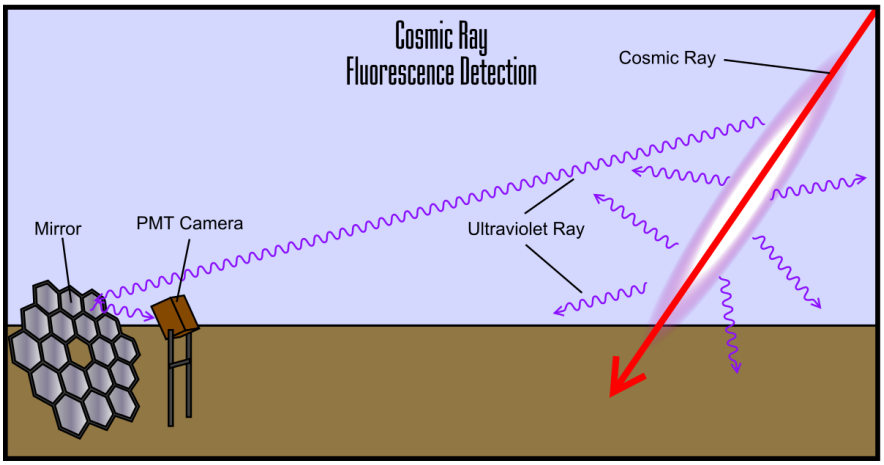

Figure 2.5: Fluorescence detector from [9].

To conclude with the description, it can be worth saying that the latter is characterized by a high angular resolution but also by a high dead time. Indeed, PMT can only be used during moonless nights to avoid blinding them with moonlight. For the same reason, it cannot be used during daytime to not blind it with sunlight.

Talking about PMT, a latency time should also be considered. This is the sum of a rise time in which photo-electrons are produced, and a fall time at the end of which the PMT is again empty. Overall, it is the interval time needed for an electron to transverse completely the tube [33]. This interval varies a little every time an electron transverse it. In fact, the interval not only depends on the dynodes' geometry and shape but also on the path the photo-electrons follow inside the tube. Few examples of the latency time of typical PMT are reported in Table 2.2 together with the Transit Time Spread (TTS) which represents the dispersion due to the variability of the path followed by the electrons in the tube.

Table 2.2: PMT time characteristics from [33].

Type	**Latency time [ns]**	**TTS [ns]**
Linear-focused	16 to 50	0.37 to 1.1
Circular-cage	57 to 70	3.6
Fine mesh	15	$<$0.45

A real infrastructure based on this methodology was Hi-Res, decommissioned around 2010. It was located in Utah, USA, and was overall composed of 64 mirrors and 256 PMT.

Both the Agasa and the latter detector analyse only one aspect of the EAS. Therefore, it has to be taken into account that their measurements may be affected by systematic errors since the shower is studied only partially.

The new generation of telescopes couples fluorescence detectors and ground arrays. Examples of the latter are the Auger in Argentina and the Telescope Array in Utah.

The first one covers an area of 3000 km^2 and is provided with 1600 Cerenkov detectors equally distanced about 1.5 km from each other, and 4 fluorescence detector stations each composed by a mirror focusing the photons on an array of 440 PMT. With this telescope, it was possible to confirm the GZK cut-off. Indeed, among all the recorded events none of them overcame $5x10^{20}$ eV [9].

The second telescope is the northern counterpart of the Auger. It is composed of 500 plastic scintillators located at 1.2 km from each other and three fluorescence stations spread over an area of just 740 km^2. Nonetheless, even in this case, the GZK' cut-off has been confirmed and the primaries have been recognized to be mainly protons and Fe nuclei [9].

2.3.2 Modern Techniques

Along modern techniques are pointed out all the brand-new methodologies that rely mostly on the investigation of the traces left in the soil by the secondary particles generated in the EAS.

In particular, the focus is on the ones produced by the hadronic shower and specifically on muons for the reason stated in Section 2.2.

As it is reported in the previously mentioned section, these particles can penetrate deep in the crust and interact with the crossed nuclei consequently leaving a trace that can be visible even many years after the passage.

In particular, the trace left by a muon is expected to be either an isotope or a damage in the crystalline structure.

Indeed, the trace can regard both the nucleus of an atom or the lattice of a crystalline structure.

In the first case, the interaction takes place at the nuclear level. In particular, it is a fission reaction. Nonetheless, because the reaction is supposed to occur at high energy, it is usually referred to as spallation. Basically, the latter entails that the hit nucleus ejects particles such as neutrons and protons [5]. The resulting nucleus is lighter than the original one. An isotope has been produced and can be either stable or unstable - radioactive. To understand the basics of this process refer to Fig. 2.6.

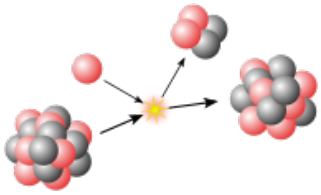

Figure 2.6: Spallation scheme from [9].

Among the isotopes produced by the passage, the radioactive ones that are characterized by a long decay time, are of interest. As a matter of fact, not all of the radioactive isotopes have a long enough lifetime to be still observable nowadays. Usually, the ones characterized by a long half-life are the heavier ones and require very high energy as well as heavy original nucleus to be formed.

In Table 2.3 are reported some of the radioactive isotopes with a sufficiently long half-life to be likely found nowadays. The possibility to discovery any of them in the outcome of the simulations developed in this project cannot be excluded a priori.

Table 2.3: Radioactive isotopes with a mean life above 100 000 years from [17].

Isotope $^{A}_{Z}$ element	**Half lifetime [y]**
$^{10}_{4}$Be	1.5 x 10^{6}
$^{40}_{19}$K	1.28 x 10^{9}
$^{144}_{53}$Nd	2.3 x 10^{15}
$^{235}_{92}$U	7.1 x 10^{8}
$^{238}_{92}$U	4.5 x 10^{9}

The particles ejected during the spallation process to produce the isotope can leave a trace too. However, these traces are rarely observed. Hence, they are not investigated here.

In the second case, the high energy particle hits an atom in a crystal lattice. In particular, the latter is an elastic collision and it occurs in such a way that the energy of the impacting particle is partially transferred to the hit atom. As a consequence, if the energy is very high, the atom is kicked out from its original position. In its place, a vacancy is left. Instead, the muon, which may still have some energy, can interact with more atoms even of different crystalline structures. Anyway, the energy of the impacting particles decreases at each collision until the particle is no more able to interact with any other surrounding atom.

This process is better known as nuclear recoil. The just described process is also reported in Fig. 2.7.

The muons produced in an EAS are energetic enough to disrupt the crystalline structure hitting it. Therefore, by studying the vacancy left in the lattice, it is possible to reconstruct the type of impacting particle.

It is important to understand that, basically, the traces left in the crystal - the vacancies - are equal to the ion tracks in a generic solid. For this reason, they can be studied through chemical etching which is a technique often exploited to track the traces left by ions.

Truthfully, this technique is necessary for this study. Indeed, the muon traces are too tiny to be actually visualized and studied directly.

For what concerns etching, it is a quite versatile technique. Indeed, it can be used with several types of solids such as crystals, glasses and polymers.

Briefly, the technique requires the immersion of the spoiled solid - the one crossed by the particle - into a chemical solvent which attacks specifically the tracks left in the lattice [34]. Indeed, it has been observed that these are much more reactive than the untouched material.

By immersing the samples, the so-called etch figures are created. These can be easily studied employing an optical microscope.

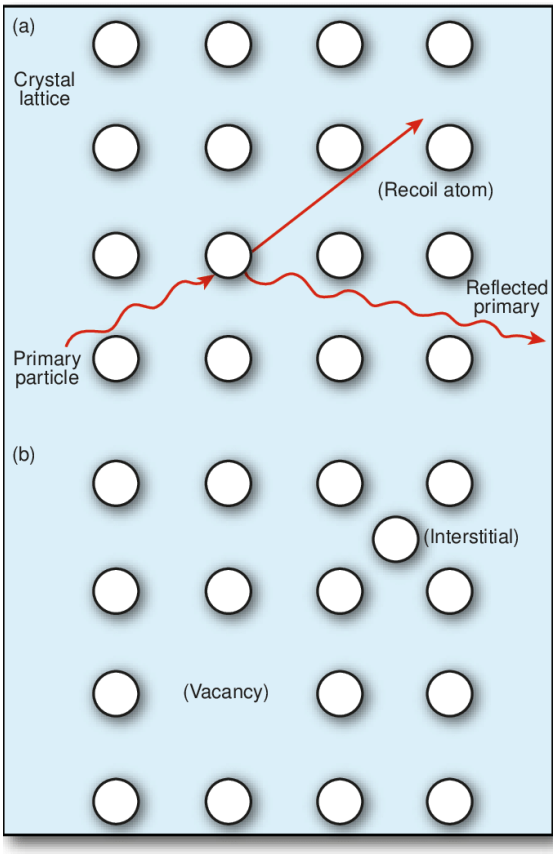

Figure 2.7: Displacement damage of a crystalline structure from [24]. a) Passage of a very energetic particle. This is supposed to have transferred enough energy to hit an atom to displace it. b) The deformed crystal lattice. It is possible to observe the vacancy defect. Indeed, the atom has moved due to the transferred energy into an interstitial position.

Nonetheless, it should be taken into account that the reactions occur only with the surfaces in contact with the solvent [12]. Consequently, any internal trail would not be detectable with this methodology.

Chapter 3

The Environment

This chapter introduces the environment in which the physical processes take place.
As mentioned in the introduction, two different situations are analysed:

- A realistic passage of a $\mu+$ through different layers.
- A direct interaction between a sample and a particle. As it is presented afterwards, the latter can be either a muon or a neutron.

These are referred to as the first and the second case study from here on out.
The aim and the development of the simulations are fully explained in a dedicated chapter, namely chapter 4. Indeed, the sole purpose of this chapter presented here, is to introduce the background in which the processes occur.
The first case study's environment is covered in Section 3.1 where the definition of a real scenario composed of two layers, one of ocean and one of oceanic crust, is provided. In Section 3.2, instead, two minerals are defined. These are used for the direct interaction analysis.

3.1 Real World

In this section, the scenario for the first case study is introduced.
Considering that the study is set to simulate realistic interactions between the particle and the surrounding matter, the environment has to be inspired by a real Earth's location.
However, the Earth is a complex dynamic system. For the sake of clarity and to not overload the simulation, it has been decided to consider only two layers: one of seawater and the other of oceanic crust. The latter is considered to be composed mainly by basalt. The reason for this choice is well explained in Section 3.1.2. The ocean is described, instead, in Section 3.1.1.
Accordingly, the $\mu+$ motion is considered to start directly from the ocean's surface so that the interactions occur only with the water and the crust.
Sure enough, it could be suggested that the particle would have to pass throughout the atmosphere before reaching the ocean's surface. Nonetheless, this part of the path has already been analysed in previous studies and for this reason is neglected here.
Furthermore, the fluxes of both muons and neutrons at sea level are known. Therefore, exploiting these measured data, it is already taken into account that some energy is dissipated in the atmosphere.
To conclude, the main interests of this analysis are the nuclei formed in the crust. Therefore, neglecting the atmospheric layer and considering the occurrence of energy loss should not overly affect the result.

3.1.1 Ocean

The Earth's surface is mostly covered by water: the ocean. The latter contains the majority of H_2O of our planet. However, several dissolved substances are mixed with it such as salt. Indeed, one of the main parameters through which the oceanic water is qualified is the salinity or rather the salt quantity in a solution. As may be expected, this parameter is not constant worldwide but changes from place to place affecting the seawater composition. In this context, the latter has

been defined for the average salinity which is about 35 g/l [35] as it is reported in Table 3.1 [35].

In addition to the chemical composition, to completely define the simulation environment at least two other pieces of information are required. The first is the density, which is 1026.02 kg/m^3 and the second is the depth. From literature, the ocean's depth results to be on average about 3.70 km [29]. This data is the one used within this framework.

Table 3.1: Ocean elemental composition from [35].

Element	**Composition [%]**	**Symbol**
Oxygen	85.84	O
Hydrogen	10.82	H
Chlorine	1.95	Cl
Sodium	1.08	Na
Magnesium	0.1292	Mg
Sulfur	0.091	S
Calcium	0.04	Ca
Potassium	0.04	K
Bromine	0.0067	Br
Carbon	0.0028	C

3.1.2 Crust

The Earth's crust is the upper layer of the lithosphere. It can be split into an oceanic and a continental part. Albeit the crust is entirely made of igneous rock, some differences in the chemical composition are present between the two [21]. For instance, the oceanic crust has a higher concentration of magnesium and iron (mafic rocks) while the continental one is richer in elements such as silicon, oxygen, aluminium, sodium, and potassium (felsic rocks) [7][6]. This is mainly due to the formation process. Indeed, mafic rocks are formed from low viscosity lava rapidly cooling, while felsic ones are made from more viscous lava [21]. Examples of rocks for each type are basalt (mafic) and granite (felsic).

Considering that the particle is supposed to cross the ocean to reach the crust, it is clear that the part of the lithosphere of interest for the analysis carried out in this project is the oceanic one.

In comparison to the continental crust, the oceanic one is younger and thinner. Moreover, it is formed in correspondence of the mid-ocean ridges and near-ridge seamounts and spans for 3-10 km of depth [32]. Along with this distance, three layers have been defined on the base of the crystalline structure of the rocks composing them.

As a matter of fact, from the surface to the inner part, the crystalline structure becomes more and more distinguishable. Indeed, the upper one, usually identified as mid-ocean ridge basalts, is composed of basaltic lavas, while the last one contains Gabbros which are coarse-grained rocks. This difference is due to the cooling process: the faster it is the finer are the grains and vice-versa. It is clear that deeper in the crust, a longer time is needed for the lava to solidify and for this reason more coarse-grained rocks are formed.

Within this analysis, the oceanic crust is modelled as a 1 km depth layer of basalt. The latter choice is led by the fact that no specific data on the oceanic crust composition have been found. Nevertheless, considering a basaltic layer of 1 km should be a good first approximation. As mentioned earlier, the upper layer is composed of lava made of basalts and also the overall crust is almost chemically equivalent to this rock. Furthermore, the model for the simulation considers only 1 km of depth. This allows to assume the uniformity of layer of rocks and to retrieve the basalt chemical composition and density. The first is reported in Table 3.2 while the second results to be 3 g/cm^3 [2].

Table 3.2: Basalt composition from [2].

Molecules	**Composition [%]**	**Symbol**
Sylicon dioxide	49.97	SiO_2
Titanium dioxide	1.87	TiO_2
Aluminum oxide	15.99	Al_2O_3
Iron(III) oxide	3.85	Fe_2O_3
Iron(II) oxide	7.24	FeO
Manganese(II) oxide	0.20	MnO
Magnesium oxide	6.84	MgO
Calcium oxide	9.62	CaO
Sodium oxide	2.96	Na_2O
Potassium monoxide	1.12	K_2O
Phosphorus pentoxide	0.35	P_2O_5

3.2 Minerals Samples

In this section are introduced the samples for the second case study. In particular, two minerals are used.

One of these is selected among the minerals composing the oceanic crust to have some continuity with the first case. Indeed, the former can be characterized in terms of either chemical composition, as it is done in the previous section (Table 3.2), or mineralogical one.

For what concerns the latter, the oceanic crust is composed of several minerals. Among them, halite is the most common and, for this reason, it is chosen as one of the samples.

The second choice felt on a rarer mineral called morenosite. Although it is not found in the oceanic crust, it screens quite well neutrons. Hence, it is considered a suitable paleodetector. Moreover, it is present in the nickel mines in the Sudbury area, Canada. This is of particular interest since that area has been involved in a meteorite impact about 1.85 billion years ago. Indeed, this knowledge allows to quite precisely date the minerals found in the former area which is useful for studies on paleodetectors.

Furthermore, both selections are made in compliance with another study on the same subject. Indeed, in this project `Geant4` is used and relevant data can be recovered to help the development of the other study too.
In Section 3.2.1 and Section 3.2.2 a full description of the two minerals can be found.

3.2.1 Morenosite

Morenosite with the chemical formula $NiSO_47(H_2O)$ is a mineral belonging to the epsomite group. It is distinguishable by its apple green colour and it is most commonly found in the continental crust. In particular, it is a secondary mineral. In fact, it derives from the nickel-bearing sulfide ores alteration.
For its characterization, both the chemical composition and the density are required. The former are reported in Table 3.3 with the relative stoichiometric coefficient, while the latter results to be 2 g/cm^3 [27].

Table 3.3: Morenosite chemical composition from [27].

Elements	**Symbol**	**Stoichiometry**
Nickel	Ni	1
Sulfur	S	1
Oxygen	O	11
Hydrogen	H	14

3.2.2 Halite

Composed of sodium and chlorine (chemical formula NaCl), halite is nothing but the typical kitchen salt. It belongs to the mineral group named after it, the halite group. It is the product of several processes such as the evaporation of huge blocks of salty water or bedded sedimentary deposits. It has an isometric crystalline structure and is usually transparent.
Its chemical composition is reported in Table 3.4, while the density is about 2 g/cm^3 [26].

Table 3.4: Halite chemical composition from [26].

Elements	**Symbol**	**Stoichiometry**
Sodium	Na	1
Chlorine	Cl	1

Chapter 4

Simulation

In this chapter, the code and the software used for the simulations are described. Moreover, the scenarios anticipated in the introduction are exhaustively explained.
The code is implemented in C++ exploiting GEANT4. This is a particular software and for this reason, deserves to be adequately introduced as it is in Section 4.1. For what concerns the code structure, it is composed of a main and several distinct files each having a specific functionality. In Section 4.2 a full description of the latter is available.
Instead, the full description of the scenarios simulated and studied in this work is available in Section 4.3.

4.1 Introduction To GEANT4

In this section, a brief introduction to GEANT4 is given.
GEANT4 is a software released in 1998 as an evolution of GEANT3. It is the result of a worldwide collaboration, subsequently called GEANT4 collaboration, which has the CERN as one of its main leaders. As a matter of fact, the latter already owned the GEANT3 version for their experiments [1].
GEANT4 is essentially a toolkit implemented in C++. This programming language is quite common and different source code editors are available. In this study, Microsoft Visual Studio has been adopted.

The ultimate goal of the GEANT4 collaboration has been the development of a flexible simulation program based on the existing GEANT3 one. To achieve this result, modern computing techniques have been investigated and finally an Object-Oriented Technology (OOT) [1] has been selected.
The latter technique has been preferred since it allows to have a flexible, clear and modular simulation environment which makes GEANT4 well-suited for particles simulations and allows its use in different fields such as Space science or medical physics.
By downloading GEANT4, a lot of functionalities are at the user disposal. These allow setting a broad range of features in the simulations such as the detector or the particles. Indeed, the former can be completely customized in terms of shapes, geometry and material, and this is true also for the particles and the processes in which these are involved. However, sets of physics lists and processes are already provided by GEANT4 and can be employed directly by the user. Moreover, functions to interact and visualize the simulation are available. For instance, several visualization methodologies are accessible in GEANT4 and the final choice on which of them to adopt depends also on the user operating system.
From the design, it has been required to have an accessible and easy tool. For this reason, a modular architecture has been employed. The result is that the functionalities of GEANT4 are partitioned into smaller independent logical units called classes which can be used either separately or in combination.
For instance, three classes are mandatory to be implemented by the user. These are [14]:

- `G4VUserDetectorConstruction`.
- `G4VUserPhysicsList`.
- `G4VUserPrimaryGenerator`.

The peculiarity of these classes arises from the fact that they are purely abstract, which means that there is no default setting for them, and the relative concrete class can be defined only by the user itself [1].

Along with these three mandatory classes, other 5 optional classes can be introduced [1]:

- `G4UserRunAction`.
- `G4UserEventAction`.
- `G4UserStackingAction`.
- `G4UserTrackingAction`.
- `G4UserSteppingAction`.

Three of them have been used within this project. A description of their role is given in Section 4.2. In general, these optional classes can be exploited to reset the default GEANT4 behaviours thereby furtherly customizing the simulation.
To conclude the discussion, a brief overview of the modular structure is given [1]. Basically, a simulation consists of a run. In each run either one or a set of events are initialized. The latter generates the first particles which pass through the detector where the physical processes occur.
To carry out all these steps, different modules are needed, namely:

- Events - to generate the first particles.
- Geometry - to define geometrically the detector structure and allow the propagation of the particles through it.
- Tracking - to move and give action step by step to the particles through the geometry.
- Physics - to define the type of action that can occur.
- Particles and materials - to define the materials of the geometry adopted and the physical properties of the particles.

Notice that both the mandatory and the optional classes are implemented in relation to these modules. An example of that is given in the following section with the description of the code implemented for this project.

4.1.1 Object-Oriented Technology

Before proceeding, it is worth spending a few words on the OOT to better understand the GEANT4 functioning.

According to the Gartner Glossary definition [15], an OOT is a model to design software whose objects contain both the data and the instructions through which it is possible to operate on the data.

In general, the OOT is developed following three main phases: the Object-Oriented Analysis (OOA); the Object-Oriented Design (OOD); the code implementation.

This development process allows to split and shrink the built software into smaller parts. The result is a set of independent functions that can be realised individually. These can also be refined through both logical and physical models whose processes are already given with, respectively, OOA and OOD.

In particular, GEANT4 is built on the Booch method. The latter allows separation into micro and macro processes of the simulation architecture. Another peculiarity of this approach is that it can be iterated and incremented at each phase. As a matter of fact, the two mentioned processes - micro and macro - are needed since each of them deals with a part of this scheme. For instance, the micro is the framework in which this approach is carried out, while the controlling framework is represented by the macro.

Furthermore, the Booch method has an additional phase with respect to the general OOT methods. The first step provides for the collection of the users requirements. Accordingly, a dummy detector simulation has been initialized during the preliminary design phase of the GEANT4 toolkit. This has been shared with users to understand whether it suited their requests or not. Once a worldwide agreement has been achieved, the model followed the step common to any OOT for the development of GEANT4.

4.2 The Code

In this section, the structure of the code implemented for the analysis related to this project is illustrated.
As already mentioned in the previous section, GEANT4 works by classes. It has been decided to follow the same scheme in the implementation of the simulation. Therefore, each of its aspects has been split into the related class and developed in a dedicated file. For instance, the mandatory class `G4VUserDetectorConstruction`, which is needed to implement the detector's geometry and material, is fully developed in the DetectorConstruction.cc file as it is better explained afterwards.
The .cc file is always complemented by a .hh header as indicated in the GEANT4 user manual [14]. Each of the .cc and .hh couple refers to a unique class. For the sake of clarity, hereafter any functional subdivision between the two is neglected and only the class's objective is analysed. Henceforth, the files are denoted only by their file's name without specifying if they are related to the main code or the header file.
To finally introduce the code, it is important to know that the GEANT4 first basic example has been taken as a reference for the implementation.
To run effectively the code, the aforementioned mandatory classes are complemented with three of the optional classes. Therefore, the complete implemented set within this project is:

- `G4VUserActionInitialization`.
- `G4VUserDetectorConstruction`.
- `G4UserEventAction`.
- `G4VUserPrimaryGeneratorAction`.
- `G4UserRunAction`.
- `G4UserSteppingAction`.

Notice that the `G4VUserActionInitialization` has not been reported in the previous section. As a matter of fact, more classes are included in the GEANT4 library that have not been stated earlier. This is because this toolbox is always in evolution and, thus, it may be difficult to keep up with the updates. Moreover, there are lots of classes available and the aim of Section 4.1 has not been to present all of them, but to give a general overview of the simulation program functioning.

Focusing back on the formerly listed classes, these are associated with a couple of .cc and .hh files. These are called just as the class implemented within and each has a specific role in the run.

Even so, some of them are interconnected. For instance, to start the run the EventAction is needed as well as the RunAction and the SteppingAction. In particular, the RunAction and the EventAction are related to the definition of the start and the end of the actions for each run. Instead, with the SteppingAction, it is possible to customize some behaviours at each step.

As already mentioned, the structure follows for simplicity the one of the exampleB1 delivered with the GEANT4 library. Hence, it is possible that some of the steps taken are not strictly fundamental for this project. In fact, GEANT4 is used only to retrieve the data related to the passage of the particles. Subsequently, the analysis of these data is performed exploiting PYTHON and MATLAB.

In the ActionInitialization, all the aforementioned files needed for the run are called back alongside the PrimaryGeneratorAction. In practice, the ActionInitialization collects all the classes needed to effectively start a working simulation. In fact, this is one of the files recalled also from the main together with the DetectorConstruction one.

The latter, just as the PrimaryGeneratorAction, deserves to be discussed more thoroughly. However, before doing so, it is fundamental to point out the absence of one mandatory class, namely `G4VUserPhysicsList`. This class is needed to introduce the physics models in the simulation.

In this context, the class is missing since a built-in physics list is employed. Specifically, `G4VModularPhysicsList` is the class used to get the QBBC library

which is the one suggested to study electromagnetic and hadronic processes.
At this point, it is possible to concentrate on the two previously mentioned files: the PrimaryGeneratorAction and the DetectorConstruction.
The first is the file in which the particle to start the simulation is defined.
It is already clear from the introduction that this work focuses on the interaction of muons ($\mu+$) with the surrounding matter. Therefore, these particles are implemented in the PrimaryGeneratorAction file.
On top of that, in the second case study, part of the simulations are carried out with neutrons instead of muons. Consequently, also these particles are defined in the former file. The reason why neutrons are simulated is better explained in the related case study (Section 4.3.2).
The selected primary particle has to be defined in terms of energy, momentum direction and initial position. For clarity, the first is specified within each case study since different ranges are considered. The momentum direction, instead, is always set as (0,0,-1) while the initial position depends on the scenario under study. For instance, in the first case study, the particles enter from a specific user-defined position at the top of the ocean. In the second one, instead, the entrance is chosen randomly by GEANT4 within a certain selected area at the top of the mineral. This choice is more accurately examined in each case study section.
Finally, the DetectorConstruction. As can be suggested by the name, this file deals with the creation of the environments. These are the same introduced in chapter 3.
The implementation of a detector is carried out defining first the logical volume and then the physical one. When the detector is at the logical volume step it is completely defined in terms of material and shape. The physical volume is needed, instead, to spatially position it. Usually, this is done about a mother volume called world.
The world defines the outermost envelope of the environment and contains all the elements needed for the simulation which are the layers of ocean and basalt for the first case study, and the minerals for the second.

To set the logical volume, the materials have to be already defined. These are implemented according to the chemical composition reported in chapter 3. The only exception is for the world volume which has been decided to fill with air, retrieved from GEANT4 library.

To complete the logical volume definition, the geometry has to be set. The reference frame used is (x,y,z) where x and y identify the surface and z the depth. On the one hand, the ocean is set to 3.7 km of depth and the crust to 1 km. These comply with what has been stated in chapter 3. Truthfully, a simulation with only 2 km of seawater has also been arranged. The reason for this is better explained in Section 4.3.1.

On the other hand, for the second case study, the minerals are sized with 1 m in the z direction. Indeed, the goal of the second simulation is to understand what are the direct interactions of a particle with a sample. Truthfully, the latter is usually of even smaller dimension than the one set here. Nonetheless, considering less than 1 m would increase the probability of no interactions vanishing the simulation scope.

The x and y directions are of lower interest for both environments. However, these values must be set in a way that prevents the particles from exiting horizontally the volume before reaching its bottom part. For this reason, the former are set to 1 km in the first case and to 1 m in the second one. Notice that, the x and y directions are always equal to each other.

The relative position to the mother volume set via the physical volume has to be defined from the geometrical centre of the smaller volumes. These are reported for each environment in Table 4.1 together with a summary of the related geometric dimensions.

Alternatively, a graphical representation of each case study is reported in the related subsection.

Table 4.1: Detectors summary.

Environment part	Position [m]	(x,y) [m]	z [m]
First case study			
Ocean	(0,0,500)	1000	3700, 2000
Basalt	(0,0,-1350)	1000	1000
Second case study			
Morenosite	(0,0,0)	1	1
Halite	(0,0,0)	1	1

4.3 Case Studies

In this section, the case studies analysed within this project are extensively explained.

The following can also be seen as a summary of the physical process and the environment. Indeed, the information given in the previous chapters is collected here and split among the case of belonging. This is believed to be quite useful since it allows to have an overall clearer understanding of the scenarios simulated in each case.

4.3.1 First Case Study

The first case study examines the interaction of a high energy particle, namely a muon, with the oceanic crust.

The latter is considered as a block of 1x1x1 km of basalt.

Before reaching the crust, however, the muon has to cross a layer composed of seawater, or rather the ocean. This is done to adjust the simulation to be as realistic as possible.

Nonetheless, it is known that the $\mu+$ is the result of the interaction between a cosmic particle and the atmosphere. Hence, depending on where it is formed, it may have to cross the atmosphere to reach the ocean's surface from which the simulation is started in this context. As previously mentioned, the atmosphere is neglected since the muon interactions with it have already been covered in other

studies. Moreover, both the muon and the neutron fluxes at sea level are known and are easily retrievable [13] [16].

The composition of the layers is available in Section 3.1.2 and Section 3.1.1, respectively for the basalt and the seawater.

The ocean is considered to be 1x1x3.7 km because 3.7 km is its average depth. Nevertheless, one simulation is also carried out considering 1x1x2 km. This is exploited afterwards to gain information on the isotopes' population generated at different equivalent depths.

A sketch of the simulation environment is available in Fig. 4.1 for the case in which the average depth is simulated.

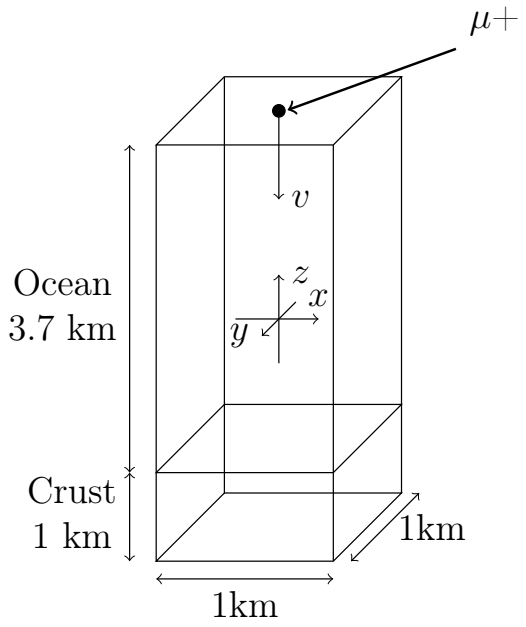

Figure 4.1: First case study geometry.

In this environment, one particle is considered to appear at the ocean's surface with a momentum direction (0,0,-1) and a certain energy.

In particular, three cases are examined. In the first one, the muon is assumed to have an energy of 10 TeV, then 50 TeV and finally 100 TeV. The results of these simulations are discussed in chapter 5.

It is worth stating the reasons for the minimum and maximum energy value choices.

On one hand, to set the lower value, several simulations have been carried out.

This process can be approximated to a reiterative one that has as stopping condition the presence of nuclei in the crust. The resulting minimum energy's value is 10 TeV. Notice that the aforementioned comparison is just to understand the process that led to the 10 TeV choice. Truthfully, this is done by testing manually different discrete levels of energy until the stopping condition is found. This implies that nuclei in the crust may be found even with energy slightly below the one chosen. Nonetheless, it is known that at 5 TeV no nuclei can be observed in the crust. This is because the muon interacts also with the salts dissolved in the water. Therefore, the energy is all dissipated along the ocean passage and the particle is not even able to reach the crust. To conclude this part, considering that with 5 TeV nothing is formed in the layer of interest, examining as a subsequent step of the iteration 10 TeV may not be a too crude approximation.
On the other hand, the choice of the maximum value is mainly related to computational time and space allocation. Indeed, on a Desktop HLL71HA with Intel(R) Core(TM) i7 the simulation with a particle at 100 TeV requires a day to finish and occupies around 100 GB. It should be taken into account that this energy value is already acceptable as maximum. Moreover, for the goal of this project, simulating three different energies should be sufficient to produce statistical data. Instead, for the case in which the ocean is 2 km of depth, only one particle with 50 TeV of energy is simulated.
The latter is chosen according to the former observation on the energy. Indeed, having 50 TeV of particles' energy allows having a substantial result in terms of isotopes produced without taking too long to be computed.

4.3.2 Second Case Study

The second case study focuses on the analysis of two minerals' samples, one of morenosite and the other of halite.
The two minerals are implemented according to their chemical composition. The latter is not reported here but can be found in Section 3.2.1 and Section 3.2.2, respectively for morenosite and halite.
Furthermore, the minerals have to be designed in terms of geometry. Both of

them have been sized as a block of 1x1x1 m as graphically reported in Fig. 4.2. The explanation for this choice can be found in Section 4.2.

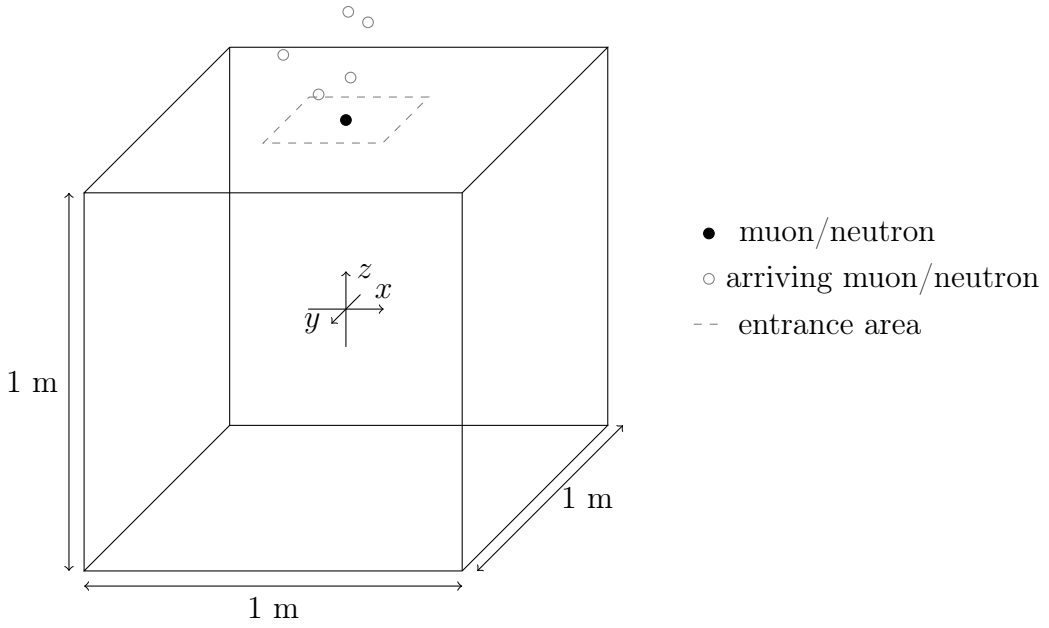

Figure 4.2: Minerals' geometry.

It could be pointed out that among the first and second case study there is no continuity, apart from halite which is actually a mineral formed by the seawater evaporation. As a matter of fact, the second case study is set in compliance with another analysis about paleodetectors. The latter focuses on the detection of the interactions of a muon and a neutron in several types of minerals. Among these, only two have been selected to be furtherly analysed through a GEANT4 simulation: morenosite and halite.

In particular, here these minerals are considered as samples collected from ancient mines and suddenly brought to the surface. Here direct interaction with particles can occur.

The analysis of this case study can be used for two different scopes, namely:

- To study the nuclei formed after the passage and understand which of them should be sought.
- To acknowledge the noise due to the particle passage once the sample is on the surface without any protection.

To figure out how the two scopes stated above relate to this analysis, it can be useful to recall the basic working principle of a paleodetector.
Till a rock is buried beneath, the layers under which it is allocated act as a shield and only certain particles are eventually able to reach it. These are usually the ones with higher energy. If the latter occurs, the particle leaves a trace in the material crossed. The types of traces produced as a consequence of the passage have been already discussed in Section 2.3.2. Hence, they are not repeated here.
On the one side, considering that the nuclei formed are not known a priori, it is necessary to simulate the passage of the particles of interest to recognize in a paleodetector sample their traces. Now it is definitely clear the reason for both the first point of the list above and the arrangement of the first case study.
On the other side, to be able to actually detect the ancient traces once the sample is on the surface, it is important to identify the latest ones and exclude them from the analysis. In fact, the most recent particles can spoil the analysis if not correctly considered. Indeed, once the rock is on the surface, the shield represented by the layers under which it was buried fail and the interactions occur with more particles. Indeed, on the surface lower energy particles such as neutrons are also present. These can interact with the uncovered sample generating new traces which represent an additional noise for the analysis. For this reason, the simulations are carried out considering not only muons but also neutrons. In addition to that, the flux is higher on the surface than in the inner part of the crust where only more energetic particles can arrive. According to that, a shower of particles is simulated.
This is done by setting a not unique entrance for the primary particle under study, but a surface on the top of the mineral and several events. In particular, 100 000 events are simulated per run which entails a shower of 100 000 particles randomly entering within the set area. The latter is the 10% of the overall top surface to allow the particles to cross entirely the detector vertically. As a matter of fact, considering the overall surface might have had as a consequence the fact that the particles exit horizontally before reaching the bottom of the sample.
Finally, also the momentum direction and energy have to be set.

The momentum direction, as for the first case study, is set at (0,0,-1). However, further refinement may also consider having a random momentum direction.
Instead, depending on the particle, different energies are considered.
In particular, the ones used in the following simulations for both muons and neutrons, are retrieved from previous studies on the fluxes of these particles.
One of the study examined to choose the energies' values [11], investigates also the primary's sources of each sub-atomic particle.
It has been noticed that, both in the muon energy's spectra and in the neutron one, the differences due to the primary particles investigated are not so relevant. The same cannot be said by comparing the spectra of the two sub-atomic particles. Indeed, the energy of the muon spreads over a wider range with respect to the neutron one. In addition to that, the former reaches also higher values. In fact, considering $E\frac{dN}{dE}$=10^5 as a landmark, the peak of the spectrum is higher than that value for the muon and lower for the neutron.
The latter is just one of the studies that have already been carried out to characterize the muons and the neutrons fluxes.
The experimental spectra used for this work are retrived from [13] and [16]. These are also available in Fig. 4.3 and Fig. 4.4 for each sub-atomic particle.

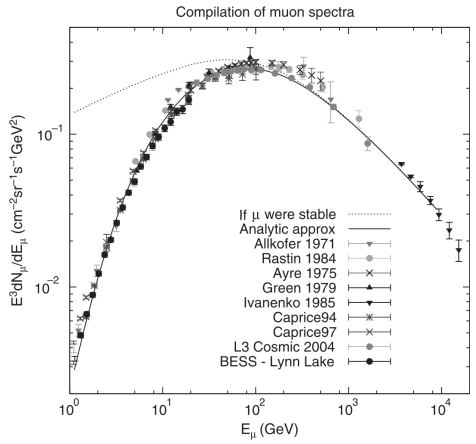

Figure 4.3: Muon experimental flux from [13].

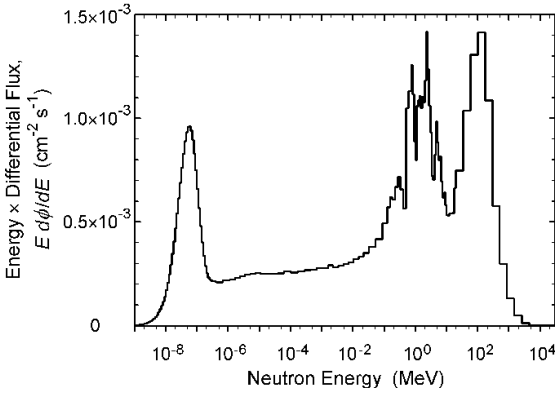

Figure 4.4: Neutron experimental flux from [16].

Accordingly, 1 GeV, 10 GeV and 50 GeV are consider as kinetic energies for the muon and 1 MeV, 100 MeV and 1 GeV for the neutron. Noticeably, the peak of each spectrum is included within these values.

Nonetheless, a further peak can be observed at a few eV for the neutron. However, only high energy particles are analysed in this study.

Chapter 5

Results

In this chapter, the outcomes of each case study shown in Section 4.3 are analysed. Three different simulations are arranged. For the sake of clarity, these are briefly reported in Table 5.1 that also provides the relative energies.

Table 5.1: Simulations summary.

Simulation	**Environment**	**Particle**	**Energies [GeV]**
1	Ocean and crust	muon	$1x10^3$, $5x10^4$, $1x10^5$
2	Morenosite/Halite	muon	1, 10, 50
3	Morenosite/Halite	neutron	0.001, 0.1, 1

Hereafter the outcomes are reported separately for each of the previous simulations. As a matter of fact, it is believed that comparing the results is useful for a further understanding of the subject. At the same time collecting them in a unique figure would overly complicate the graphical representation preventing the possibility of actually understanding them.

Therefore, all the outcomes are collected in Section 5.2 and the comparison is done by putting the relevant graphs one besides the other.

Furthermore, in the former section, the analysis of the outcomes is carried out following a well-defined scheme. First, the isotopes generated by the passages are counted and catalogued based on their weight and energy. Then, the presence of radioactive isotopes is investigated.

If any of them is found, further analyses such as the estimation of radioactive

population as well as their time propagation are carried out.
Nonetheless, before proceeding with the results, it is worth mentioning the process that led to the outcomes reported in the aforementioned sections.
Indeed, the number of data resulting from the GEANT4 simulations can be enormous and more than enough. For instance, in the first case study, the nuclei obtained in the seawater are not significant for this project. Consequently, they need to be filtered out to avoid spoiling the analysis.
The process followed to extrapolate and analyse the results is comprehensively described in Section 5.1.

5.1 Output Processing

In this section, the process through which the data are extrapolated from the GEANT4 files generated in each simulation is schematically presented.
The outcomes files of GEANT4 can require several GB. It is clear that it is complex to handle such a huge amount of data. Moreover, not all of these data are necessary for the sake of this project. The consequence is the need to both extrapolate and filter the data of interest from the overall ones.
This is particularly true for the first case study. In fact, as a consequence of the passage of the muon, nuclei are also formed in the ocean's layer. These are not of interest to this study and need to be discarded.
In practice, the data to be analysed are retrieved following three steps. These are:

1. Simulation of the passage.
2. Extrapolation of the nuclei of interest for the project.
3. Eventual filtering.

To carry out the second and third steps, differently from the first one, other types of software than GEANT4 are used. In particular, the extraction of the nuclei is executed employing PYTHON, while the filtering is performed with MATLAB. The latter is also used to plot and analyse the outcomes.

Specifically, PYTHON is executed to scan the GEANT4 outcome file and save just the necessary elements on another file. Indeed, several particles and elements are produced along with a simulation in the latter software and each of them is also complemented with a series of details more or less important.
Among all the outcomes, only some elements are of interest to this project: the ones reported in Table 5.2. These are extrapolated and saved on a new file using their name. Alongside, also the depths at which the elements are generated and their kinetic energies are kept. As it can be noticed also from the table, the nuclei are sought through their element rather than their mass. This last parameter is particularly important as it is used to identify the presence of radioactive isotopes.

Table 5.2: Elements of interest. These are the ones extrapolated from the GEANT4 file by PYTHON.

Li	Be	B	C	N	O	F	Ne	Na	Mg	Al	Si	P	S	Cl	K	Ca	Fe

Nevertheless, the data retained by PYTHON may still have to be filtered before the actual analysis. This is particularly true always for the first simulation or rather the first case study since several elements mentioned in Table 5.2 can be found also in the ocean as a product of the passage of the $\mu+$.
To exclude the latter, the file created by PYTHON is passed to MATLAB where the nuclei are filtered based on their depths. Indeed, the position of the crust in the simulation is known. Therefore, it can be exploited to understand whether the nucleus analysed belongs to it or not.
It is important to say that the processes of extrapolation and filtering could have been done exploiting the same software. Nonetheless, in this project, the use of MATLAB has been preferred. Indeed, this software has been extensively used in the past by the author of this research, leading to a deep knowledge of its functioning. As a consequence, the data were easier to be handled with it than with PYTHON, and the addition of a filtering step was not believed to increase significantly the computational effort.
The results obtained at the end of the overall extrapolation and filtering processes are finally analysed and graphically represented through MATLAB.

5.2 Simulations Results

In this section, all the results of the three simulations cited in the introduction to this chapter are gathered.
As already mentioned, the outcomes are presented following a well-defined scheme. This is:

- Counting the isotopes based on the mass.
- Cataloging each isotope based on its mass and energy.
- Investigating the presence of radioactive isotopes. If any is found, evaluate the overall population generated.
- Propagating in time the radioisotopes if any is found.

Therefore, the study starts with a broader analysis of the isotopes produced by the passage of the particles as to subsequently focus on the investigation of only the radioactive ones. Obviously, the latter entails that radioactive elements have been found among the produced isotopes.
As it has already been pointed out, the outcomes have been reported separately for each simulation as to facilitate the reading of such a huge amount of data. Indeed, in several cases, the number of isotopes retrieved during the extrapolation and filtering, is still large. As a consequence, an overlap of the outcomes would only further complicate their understanding.
Accordingly, hereunder the results are reported. Following the previous scheme, the first ones regard the isotopes population.
In the first place the isotopes of the two minerals are analysed, both in the case of the $\mu+$ and the neutron.
Specifically, the minerals are flanked on the base of the particle's type and energy. In this way, it is still possible to compare the three parameters of interest: the energy, the mass and the number of isotopes generated. The first column of figures always refers to halite and the second to morenosite.
Finally, the results related to the oceanic crust are reported.

Looking at Fig. 5.1, Fig. 5.2 and Fig. 5.3, it is possible to study the trends of the single minerals as well as their comparison.

Notice that the bar graphs are on a logarithmic scale. This is done to make the results more comprehensible but at the same time entails that the isotopes appearing only once are identified just by a grey vertical line in correspondence of their mass.

As it could be expected, the number of isotopes in each sample increases every simulation as a consequence of the sub-atomic particle's energy increment. This is true also for the energy in the case of halite. To what concerns morenosite, the kinetic energy of the isotopes drops from the first to the second simulation to increase again in the third one. This may be due to the fact that each time the $\mu+$ energy increases, the isotopes produced span over a wider range of atomic weight. Therefore, lighter as well as heavier isotopes are produced and the energy on the average decreases. As a matter of fact, even in the last case in which a re-growth of the isotopes' energy is observable, the former is true only for a few sporadic elements. Looking at the results in their entirety, it would be noticed that, on average, the energy does not grow from the second to the third simulation.

Interesting features can be obtained also by comparing the two minerals. Indeed, analysing the figures it is possible to observe that the isotopes produced in morenosite are generally lighter than the ones in halite. Furthermore, the former are in general more energetic than the latter. Truly, it is not possible to define a trend. For instance, looking at Fig. 5.1d, the maximum energy of morenosite is around 35 MeV while the one of halite is not even 15 MeV (Fig. 5.1c). Nonetheless, analysing the subsequent case reported in Fig. 5.2d and Fig. 5.2c, the results are the opposite. The maximum energy of halite is 40 MeV while morenosite barely reaches 30 MeV. In the last simulation (Fig. 5.3d, Fig. 5.3c) the trend switches again due to a sporadic value at 60 MeV in morenosite.

Moving on to the neutron passage, Fig. 5.4, Fig. 5.5 and Fig. 5.6 should be considered. As before, the results are first analysed per minerals and then compared. Differently from the $\mu+$ case, here not only does the number of isotopes increase but also the energy shows a growth trend in each mineral.

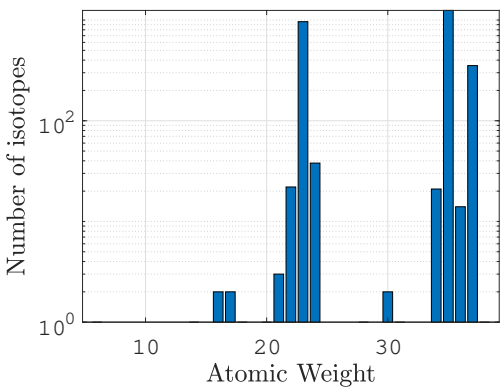

(a) Number of elements produced in halite.

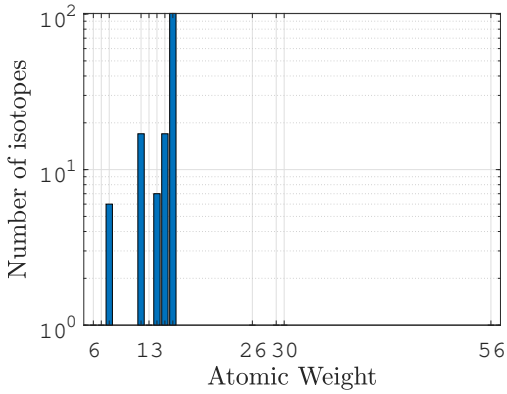

(b) Number of elements produced in morenosite.

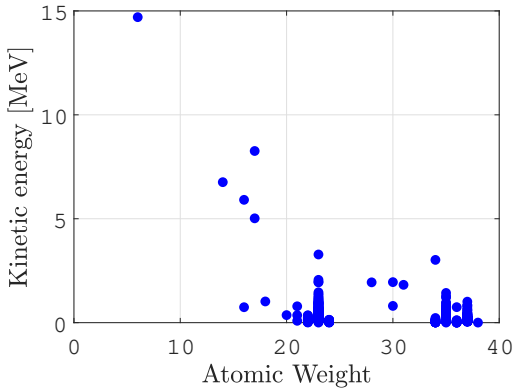

(c) Energy of the elements produced in halite.

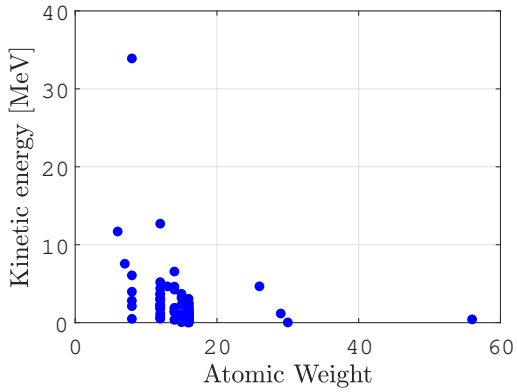

(d) Energy of the elements produced in Morenosite.

Figure 5.1: Elements produced by the passage of a 1 GeV $\mu+$.

From the comparison, instead, it is possible to highlight that the isotopes are still in general lighter in morenosite and heavier in halite. However, the atomic weight axis fills up as the energy of the neutron increases. On top of that, the mass range suddenly grows in each mineral from the first (Fig. 5.4c, Fig. 5.4d) to the second case of study (Fig. 5.5c, Fig. 5.5d). The largest increase regards morenosite in which also heavier elements around 60 of atomic weight are produced. Also halite shows a sudden production of lighter elements reaching down to nearly 5 of atomic weight. From the second to the third simulation, the ranges enlarge a little more but the increase is smoother than the earlier one. To conclude the analysis of the results of the neutron passage, it is worth mentioning one last aspect that arises from the comparison: the energy. As in the $\mu+$ case, it is not possible to define

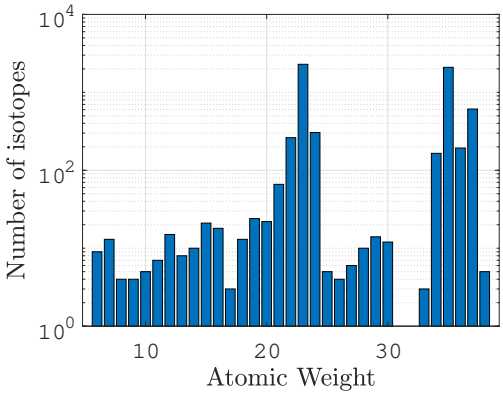

(a) Number of elements produced in halite.

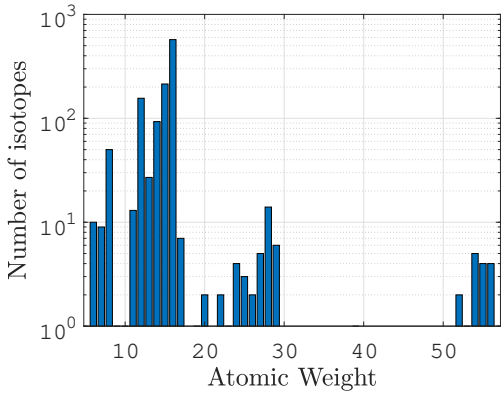

(b) Number of elements produced in morenosite.

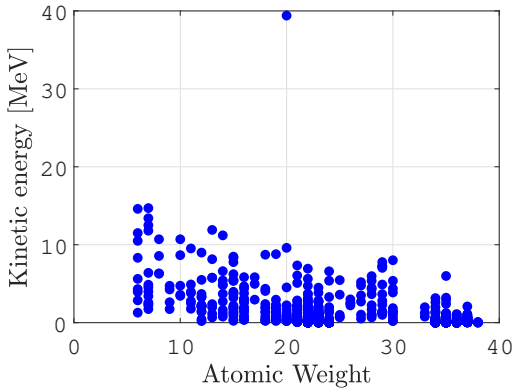

(c) Energy of the elements produced in halite.

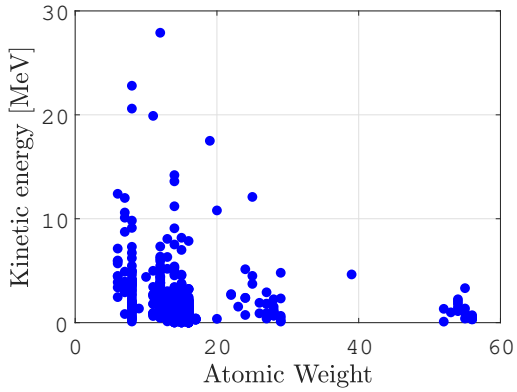

(d) Energy of the elements produced in morenosite.

Figure 5.2: Elements produced by the passage of a 10 GeV $\mu+$.

a single trend. First, morenosite has higher energy than halite; then, the values reverse and halite has the higher maximum energy. In the end, the first situation repeats. Still, this is not an analysis of the average value, but of the peaks.

Finally, the results related to the oceanic crust are analysed. These can be found in Fig. 5.7.

Just as in the previous cases, each increase of the sub-atomic particle energy corresponds to an isotope's population growth. The same cannot be said for the isotopes' energies. Indeed, the latter increases from the first (Fig. 5.7b) to the second simulation (Fig. 5.7d) to finally drop in the third one (Fig. 5.7f). However, the maximum value in the second case is due to a single isotope around 20 of atomic weight. Therefore, a growth trend would be observed if this particular

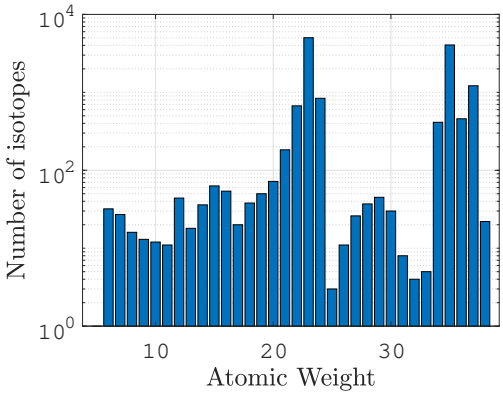

(a) Number of elements produced in halite.

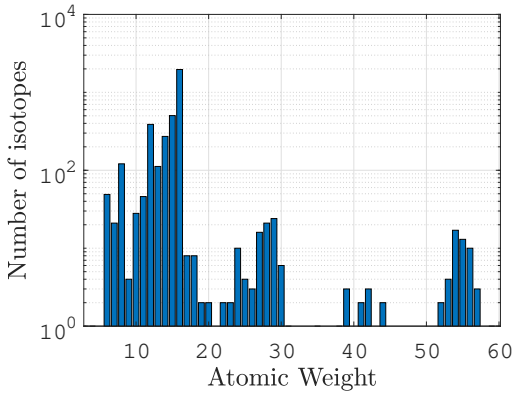

(b) Number of elements produced in morenosite.

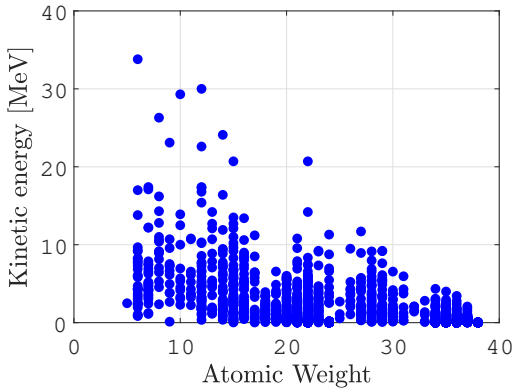

(c) Energy of the elements produced in halite.

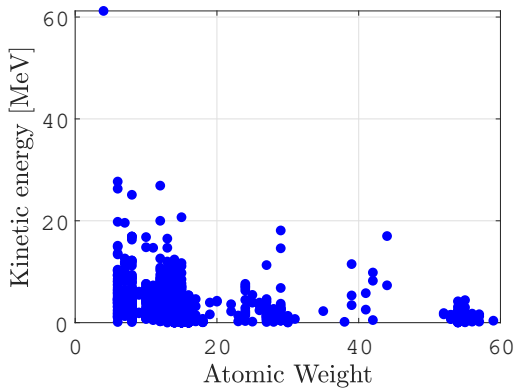

(d) Energy of the elements produced in morenosite.

Figure 5.3: Elements produced by the passage of a 50 GeV $\mu+$.

case is excluded.

Before concluding and proceeding with other analyses, it is worth observing that the atomic weight range increases from the first to the second simulation and that the elements are in general on the lighter side of the atomic weight axis.

Continuing with the radioactive isotopes' analysis, it is important to recall which isotopes have to be investigated. These can be found in Table 2.3.

In particular, two radioisotopes belonging to the former table have been found. These are, obviously, the lighter ones, namely ^{10}Be and ^{40}K.

Truthfully, there are cases in which neither of the two is present or at least one of the two isotopes is missing. As it could be expected, the latter are the simulations with a lower energy of the sub-atomic particles.

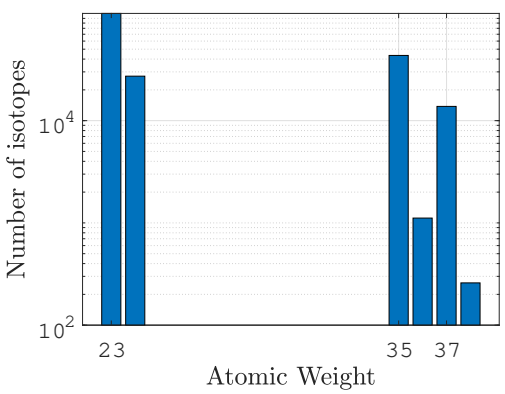

(a) Number of elements produced in halite.

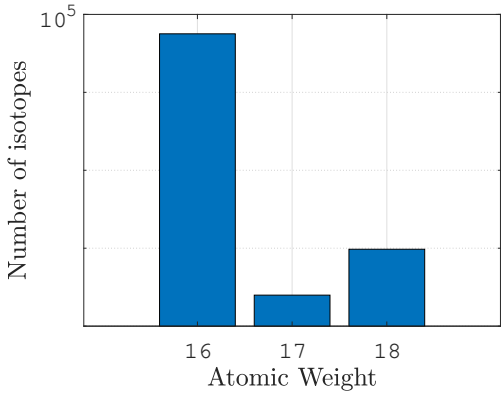

(b) Number of elements produced in morenosite.

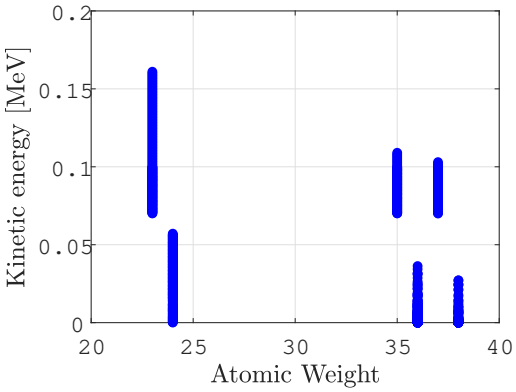

(c) Energy of the elements produced in halite.

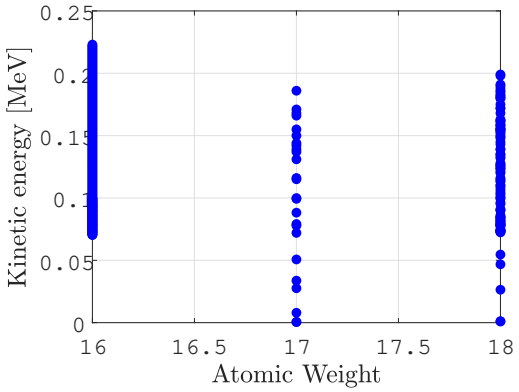

(d) Energy of the elements produced in morenosite.

Figure 5.4: Elements produced by the passage of a 1 MeV n.

However, considering six scenarios composed each by three energies of one of the two particles, the two radioactive isotopes are always observable. The values within each scenario are interpolated. In this way, the production of the radioisotopes can be analysed in function of the energy of either the muon or the neutron in each material.

Therefore, the number of isotopes are first collected per element and energy. Subsequently, these values are interpolated exploiting a built-in MATLAB command, namely `interp1`, which requires the x and y values together with the method of interpolation. Using the function handle and specifying inside the previous command the variable, an interpolating function can be generated which is useful for the sake of this project. Therefore, an N(E) function is created.

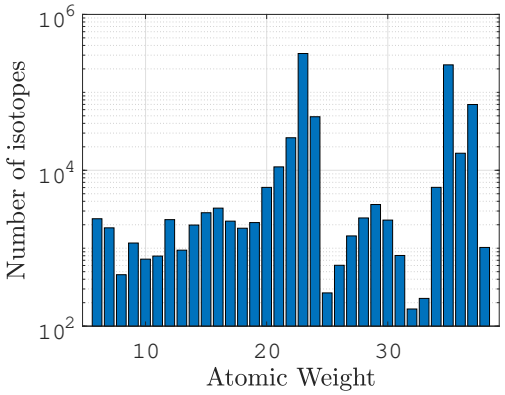

(a) Number of elements produced in halite.

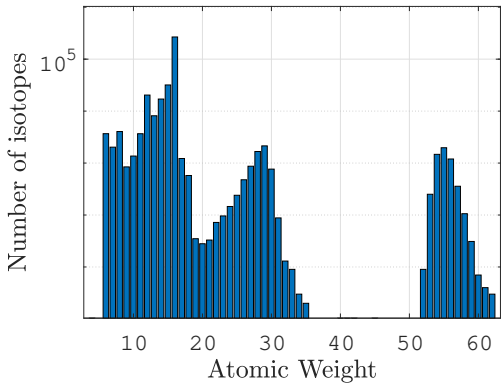

(b) Number of elements produced in morenosite.

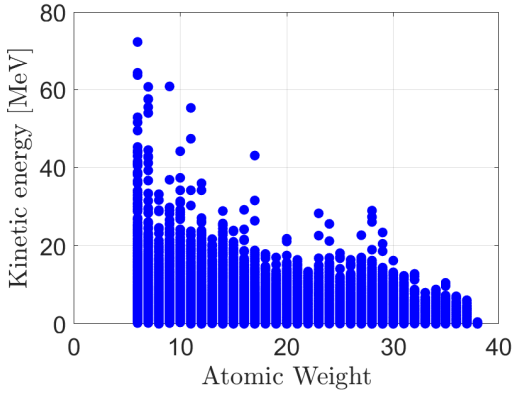

(c) Energy of the elements produced in halite.

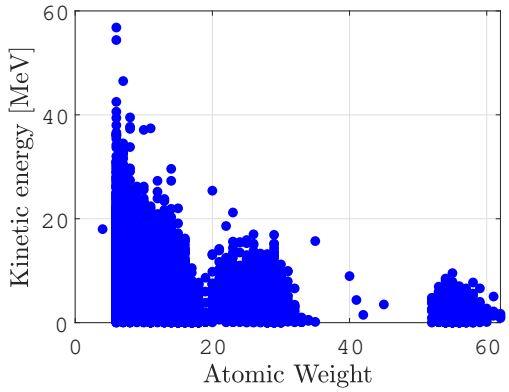

(d) Energy of the elements produced in morenosite.

Figure 5.5: Elements produced by the passage of a 100 MeV n.

The interpolation method used is `pchip`, a shape-preserving piece wise cubic interpolation [23] which produces a function continuous in C^1.

In the following figure, each N(E) function is represented over its range of energy. In particular, it is possible to observe that the ^{40}K in two cases cannot be found even at higher energy. These are the cases of the muon passage in the minerals. The fact that the ^{10}Be is still present should not be a concern. Indeed, it is more likely that this is produced rather than the ^{40}K, since it is lighter and requires less energy to be generated.

In all the other scenarios, both radioactive isotopes are present.

In addition to the evaluation of N(E), it has been decided to compute the flux of isotopes produced by the passage of either the neutron or the muon.

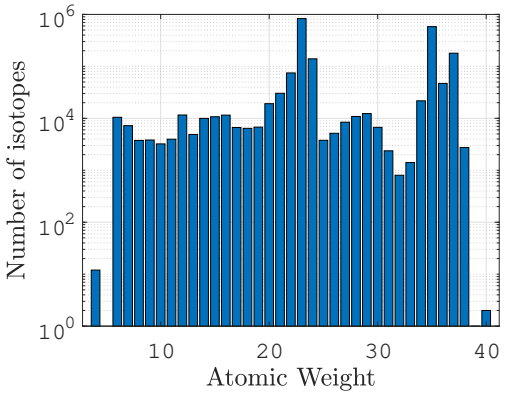

(a) Number of elements produced in halite.

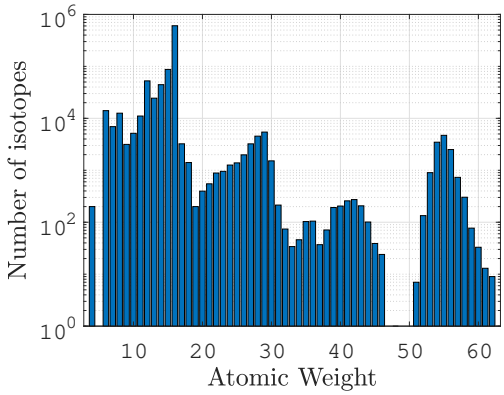

(b) Number of elements produced in morenosite.

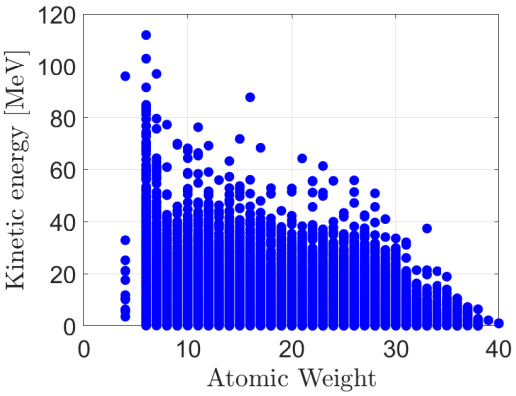

(c) Energy of the elements produced in halite.

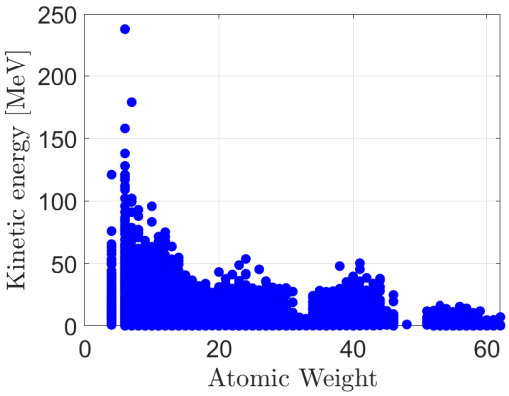

(d) Energy of the elements produced in morenosite.

Figure 5.6: Elements produced by the passage of a 1 GeV n.

To do so, the former functions are multiplied by the flux of the sub-atomic particle involved.

In particular, these fluxes are implemented extrapolating several points from the experimental ones and interpolating them through the same MATLAB command `interp1` previously used for the function N(E).

The results are available in Fig. 5.13 and Fig. 5.14. These can be compared with the measured values reported in Fig. 4.3 and Fig. 4.4.

Notice that, for the neutron flux, only the high energy range has been implemented. The reason for this choice is stated in Section 4.3.2. However, it is enough to know that the high energy peak of the flux belongs to that range to justify the choice.

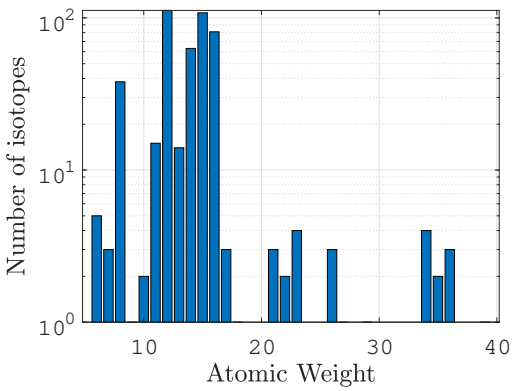

(a) Number of elements produced by a 10 TeV $\mu+$.

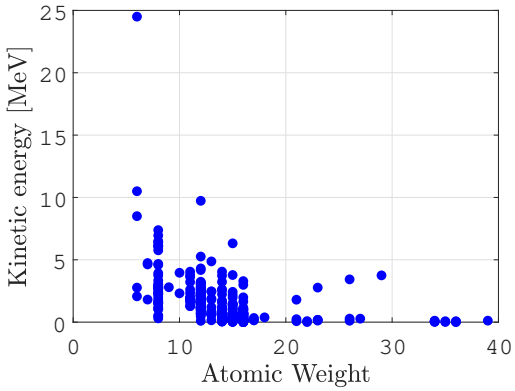

(b) Energy of elements produced by a 10 TeV $\mu+$.

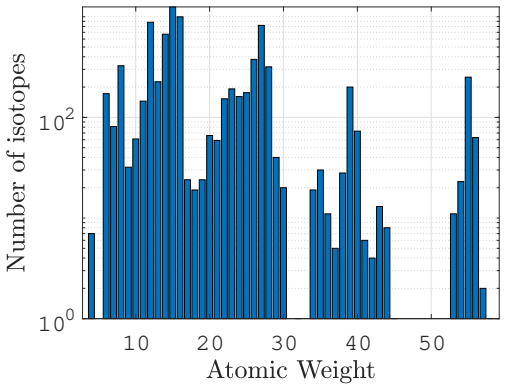

(c) Number of the elements produced by a 50 TeV $\mu+$.

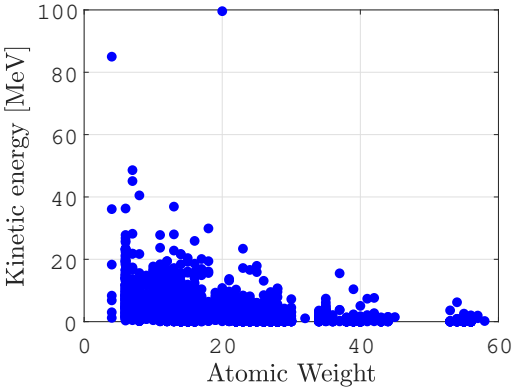

(d) Energy of the elements produced by a 50 TeV $\mu+$.

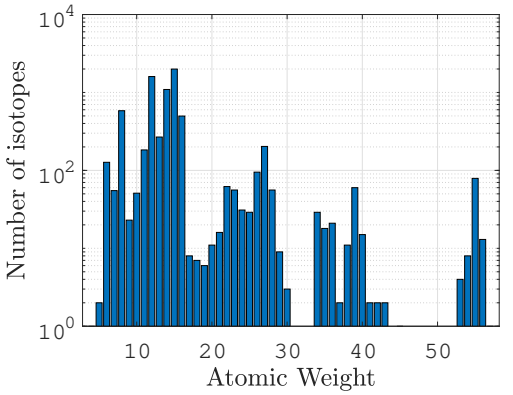

(e) Number of the elements produced by a 100 TeV $\mu+$.

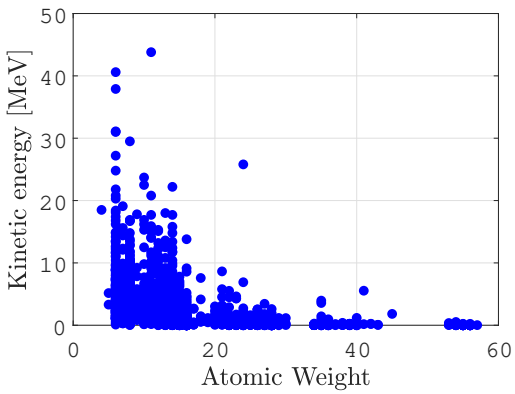

(f) Energy of the elements produced by a 100 TeV $\mu+$.

Figure 5.7: Elements produced by the passage in the oceanic crust.

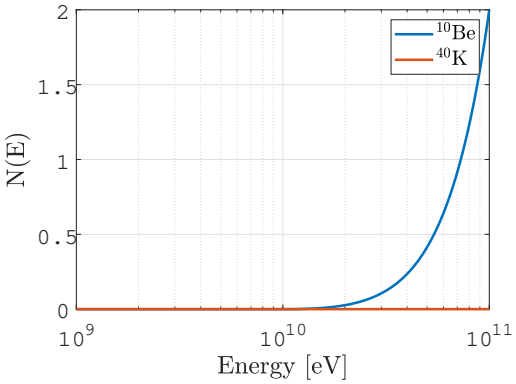

Figure 5.8: Radioactive isotopes produced by the passage of a $\mu+$ in halite.

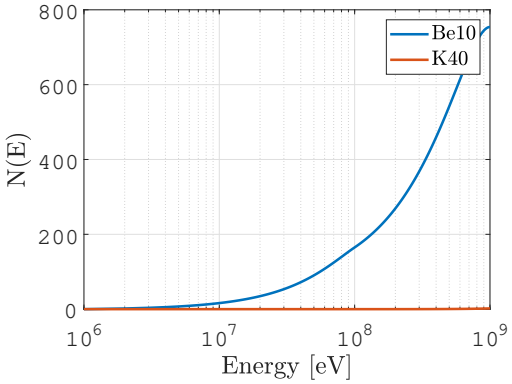

Figure 5.9: Radioactive isotopes produced by the passage of a n in halite.

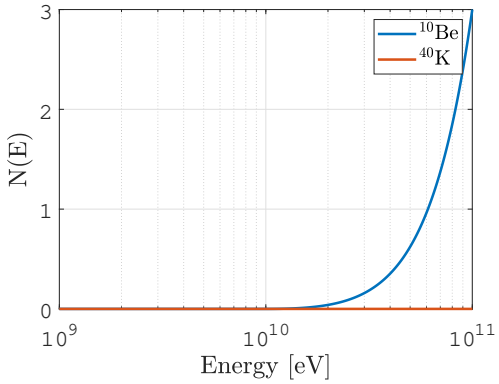

Figure 5.10: Radioactive isotopes produced by the passage of a $\mu+$ in morenosite.

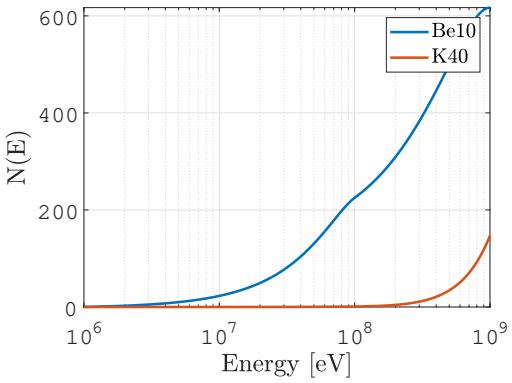

Figure 5.11: Radioactive isotopes produced by the passage of a n in morenosite.

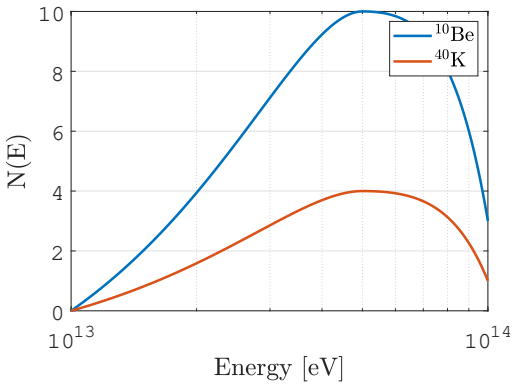

Figure 5.12: Radioactive isotopes produced by the passage of a $\mu+$ in the oceanic crust.

Truthfully, the latter are the spectra respectively of the muon and the neutron. However, the flux can be easily evaluated by dividing by E^3 the first one and just

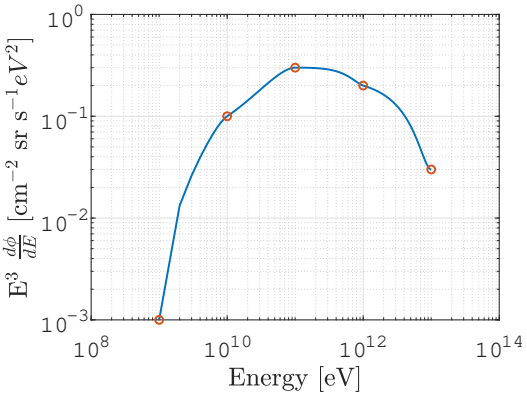

Figure 5.13: Interpolated $\mu+$ flux.

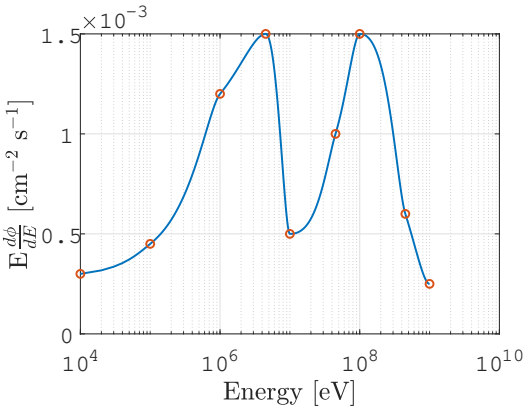

Figure 5.14: Interpolated n flux.

by E the second one.

At this point, knowing the fluxes $\frac{d\phi}{dE}$ and the isotopes production N(E), it is possible to evaluate the flux of the isotopes $\frac{d\phi_{isot}}{dE}$.

For the minerals, the latter is computed as

$$\frac{d\phi_{isot}}{dE} = \frac{2\pi}{10^5}\frac{d\phi}{dE}N(E) \tag{5.1}$$

for the muons, and as

$$\frac{d\phi_{isot}}{dE} = \frac{1}{10^5}\frac{d\phi}{dE}N(E) \tag{5.2}$$

for the neutrons.

The presence of the factor 2π in the first equation is due to the fact that the flux depends also on the angle of arrival of the muon. Multiplying by 2π the arrival directions dependence is omitted.

Furthermore, the isotopes' fluxes are divided by 100 000. This is done since the isotope's production is obtained simulating a flux of 100 000 particles. Therefore, to quantify the value for a generic flux, it is necessary to normalize the isotopes number by that factor.

The fluxes obtained with the previous reported procedure can be visually appreciated in Fig. 5.15 and Fig. 5.17 for the case in which the primary is the $\mu+$ and in Fig. 5.16 and Fig. 5.18 for the neutron case.

For the ocean, a further step is taken. Indeed, the number of radioactive isotopes

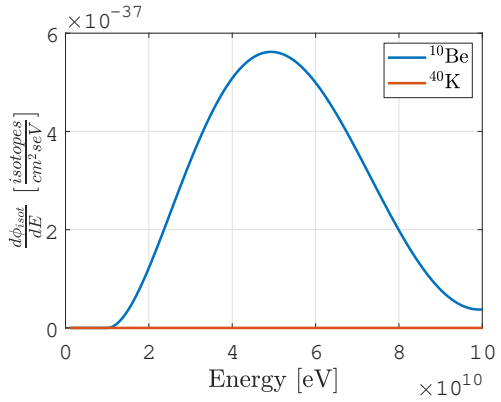

Figure 5.15: Radioactive isotopes flux produced by the passage of a $\mu+$ in halite.

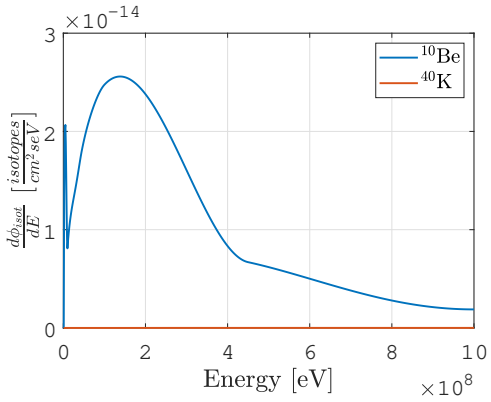

Figure 5.16: Radioactive isotopes flux produced by the passage of a n in halite.

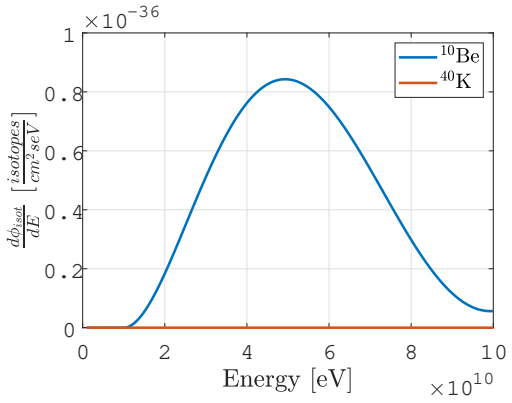

Figure 5.17: Radioactive isotopes flux produced by the passage of a $\mu+$ in morenosite.

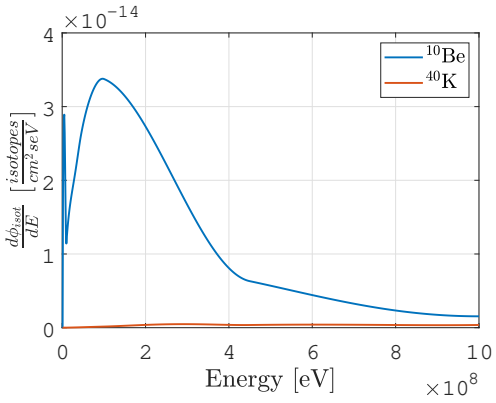

Figure 5.18: Radioactive isotopes flux produced by the passage of a n in morenosite.

produced has not been evaluated only based on the energy of the primary but also on the depth of the sea layer.

To do so, the data obtained simulating 3.7 km and 2 km of ocean's depth and 50 TeV of particle's energy have been interpolated. Differently from the earlier interpolations, this is done using the built-in MATLAB command `fit`. As a matter of fact, this command allows constructing specific functions as it is needed in this case. Particularly, the function obtained by this interpolation is required to be exponential. This is done specifying in the `fit` command `exp1` as fitType [22]. The result is called depth sensitivity function s(h) and is represented in Fig. 5.19, Fig. 5.20 and Fig. 5.21. The first represents the overall isotopes population produced by the muon passage as a function of the sea's depth. The second and the

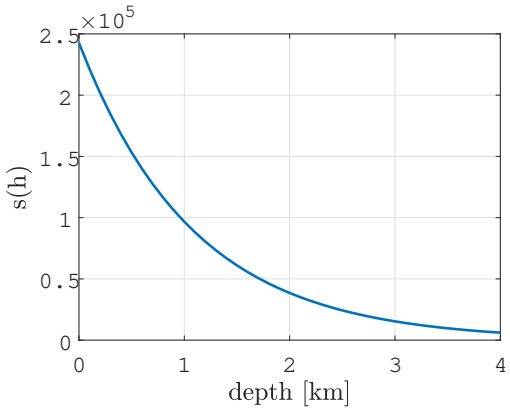

Figure 5.19: Sensitivity function: number of isotopes produced on the base of the ocean's depth.

third reports respectively the ^{10}Be and the ^{40}K in function of the depth.

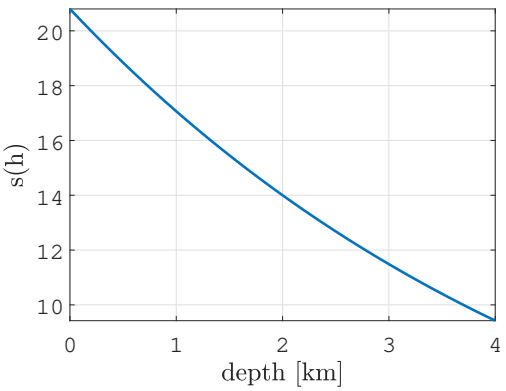

Figure 5.20: Sensitivity function representative of the ^{10}Be population on the base of the ocean's depth.

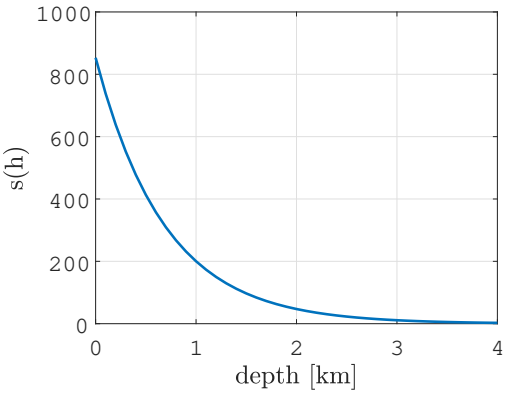

Figure 5.21: Sensitivity function representative of the ^{40}K population on the base of the ocean's depth.

Before proceeding, it is worth recalling that the simulations carried out in this project consider the incoming particles arriving always perpendicular to the surface. Therefore, to generalize the results obtained for the sensitivity function, the depth reported there should be regarded as an equivalent ocean's depth.
Referring to the scheme reported in Fig. 5.22, the actual depth can be easily evaluated as

$$h = h_{eq} \cos\theta \tag{5.3}$$

Therefore, the general sensitivity function is

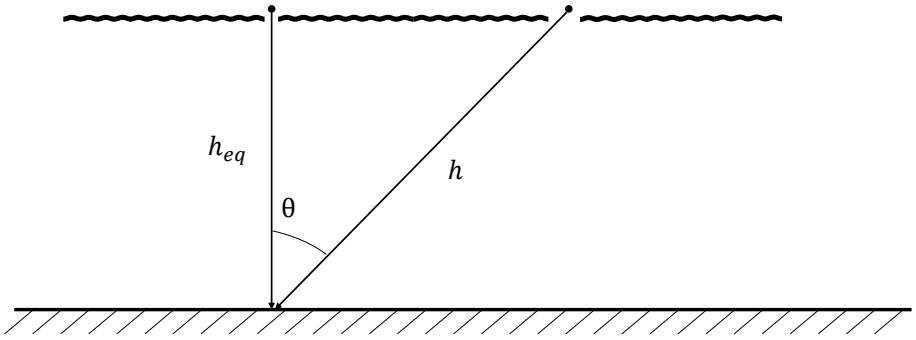

Figure 5.22: Geometry for the depth evaluation.

$$s(h,\theta) = N_0 e^{-\frac{\gamma h}{\cos\theta}} \tag{5.4}$$

The last variable that has to be introduced is the flux. In this case, it can be approximated to

$$\frac{d\phi_{ocean}(E,\theta)}{dE} = \frac{d\phi(E)}{dE}\cos^2\theta \tag{5.5}$$

where $\frac{d\phi(E)}{dE}$ is nothing other than the previously introduced muon flux.
Finally, the flux of isotopes can be evaluated as in Eq. (5.6)

$$\phi_{isot}(h) = \int_{E_{min}}^{E_{max}} \int_0^{\frac{\pi}{2}} N(E)\frac{d\phi_{ocean}(E,\theta)}{dE} s(h,\theta)\, dE d\theta \tag{5.6}$$

The result is reported in Fig. 5.23.
To conclude the analysis, the radioactive isotopes found in each case are propagated in time.
In particular, the focus is on the minerals and basalt rather than the overall radioisotopes population observable nowadays. Indeed, for the latter, additional simulations are necessary to understand the fluxes of both the muon and the neutron due uniquely to a primary particle in the high energy range.

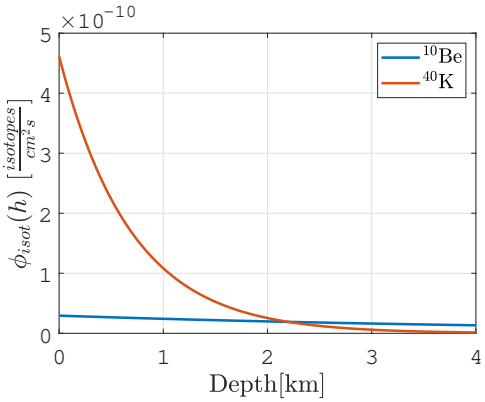

Figure 5.23: Radioactive isotopes flux produced by the passage of a $\mu+$ in the oceanic crust.

Indeed, as already mentioned, the fluxes previously used do not necessarily arise from a cosmic ray of high energy passage but are generic spectra measured experimentally at sea level.

Therefore, the radioisotopes produced in each simulation are studied in terms of saturation value and saturation time. Indeed, after a certain time called here saturation time, in each sample the number of isotopes produced by a passage balances with the decaying one. This equilibrium value has been named saturation value.

To quantify these two parameters, it has been decided to simulate a total interval time of 100 000 years. Wherein the latter, it has been supposed that every 100 years the secondaries pass through the samples producing a certain amount of radioisotopes. The initial number N_0 at each interaction is retrieved by the GEANT4 simulations.

Therefore, knowing that the decay law is

$$N(t) = N_0 e^{-\lambda t} \tag{5.7}$$

where N_0 is the GEANT4 value, t the time in years and λ is defined as

$$\lambda = \frac{\log 2}{t_{half}} \tag{5.8}$$

where t_{half} is the half-life defined in Table 2.3, it is possible to evaluate the saturation value and time.

To understand whether the population reached the plateau or not, the number of isotopes at each step has been compared with the one at the previous step. Considering a tolerance of 10^{-7}, the saturation has been considered reached when the difference between the two steps was smaller than the former value.

However, arranging the simulation as previously presented, in none of the minerals the isotopes reached that condition. Consequently, another simulation has been carried out increasing the time range to 100 000 000 years.

Nonetheless, such a simulation requires a huge computational effort and time. Hence, additional changes have been applied. One possibility to offload the simulation is an increase in the period between one production and the other. Therefore, the latter has been switched from 100 to 1 000 years first and to 10 000 after. These values have been taken arbitrarily in compliance with the typical passages' time interval of a cosmic ray of high energy. Indeed, this period spans from 1 year up to 1 century and more. Consequently, it can be supposed that each passage occurs after either 1 000 or 10 000 years.

Accordingly, two other simulations have been carried out with a total time of 100 000 000 years, and a period of production of firstly 1 000 years and then of 10 000 years. In these cases, some samples saturate.

Future development may take into consideration other ranges of time and intervals between the passages. Moreover, with a more powerful device, also the case of 100 000 000 years with 100 years between the production of the isotopes should be simulated to have a complete overview of the cases.

The results obtained are reported in Table 5.3, Table 5.4 and Table 5.5.
Indeed, even though no saturation has been recorded, the number of isotopes that can be found after 100 000 years with 100 years of span, have been reported too. Notice that, the growth can be described by a linear function. Therefore, it is enough to interpolate the reported data with a first-degree interpolation method to retrieve the intermediate values.

Table 5.3: Radioisotopes initial and final values after 100 000 years with a time span of production of 100 years.

Mineral	**Isotope**	**Part. energy**	$\mathbf{N_0}$	$\mathbf{N_{100\,000}}$
Halite	^{10}Be	$\mu+$ at 100 GeV	2	1.9564e3
	^{10}Be	n at 0.1 GeV	165	1.6141e5
	^{10}Be	n at 1 GeV	754	7.3758e5
	^{40}K	n at 1 GeV	2	2.0019e3
Morenosite	^{10}Be	$\mu+$ at 100 GeV	3	2.9347e3
	^{10}Be	n at 0.1 GeV	225	2.2010e5
	^{10}Be	n at 1 GeV	617	6.0356e5
	^{40}K	n at 0.1 GeV	1	1.0010e3
	^{40}K	n at 1 GeV	147	1.4714e5
Basalt	^{10}Be	$\mu+$ at 50 TeV	10	9.7822e3
	^{10}Be	$\mu+$ at 100 TeV	3	2.9347e3
	^{40}K	$\mu+$ at 50 TeV	4	4.0039e3
	^{40}K	$\mu+$ at 100 TeV	1	1.0010e3

The former result could lead to believe that, in the same situation, radioactive isotopes with a shorter half-life would also be observable. Consequently, future analysis of the radioactive traces produced by the two sub-atomic particles considered within this project, should investigate the presence of even lighter radioisotopes which are also more likely to be produced.
Looking at the results of the second and third cases, it is interesting to notice that each isotope that saturates does so almost at the very same time in every simulation. Certainly, the value at saturation changes since the time intervals switch from 1 000 to 10 000 years.

Table 5.4: Radioisotopes initial and saturated values and time to reach it, simulating 100 000 000 years with a time span of production of 1 000 years. Where saturation is still not reached the saturation time is defined as >100 000 000 and the saturation value is actually the population of isotopes observable after that time.

Mineral	**Isotope**	**Part. energy**	$\mathbf{N_0}$	$\mathbf{N_{sat}}$	**Time [y]**
Halite	^{10}Be	$\mu+$ at 100 GeV	2	4.3291e3	31 398 000
	^{10}Be	n at 0.1 GeV	165	3.5715e5	40 947 000
	^{10}Be	n at 1 GeV	754	1.6321e6	44 235 000
	^{40}K	n at 1 GeV	2	1.9468e5	>100 000 000
Morenosite	^{10}Be	$\mu+$ at 100 GeV	3	6.4936e3	32 275 000
	^{10}Be	n at 0.1 GeV	225	4.8702e5	41 619 000
	^{10}Be	n at 1 GeV	617	1.3355e6	43 801 000
	^{40}K	n at 0.1 GeV	1	9.7342e4	>100 000 000
	^{40}K	n at 1 GeV	147	1.4309e7	>100 000 000
Basalt	^{10}Be	$\mu+$ at 50 TeV	10	2.1645e4	32 275 000
	^{10}Be	$\mu+$ at 100 TeV	3	6.4936e3	34 881 000
	^{40}K	$\mu+$ at 50 TeV	4	3.8937e5	>100 000 000
	^{40}K	$\mu+$ at 100 TeV	1	9.7342e4	>100 000 000

The fact that the time at which the production of radioisotopes balances the decay ones is similar, may entail that each mineral is likely to saturate for a certain isotope after a certain period regardless of the production's time span. If this is true, the arrival time of a cosmic ray would become less significant for the evaluation of the radioactive isotopes. Consequently, also the generic fluxes introduced above could be used for the final evaluation of the radioisotope's population since the sources producing the secondary particles would not be any more important.

Table 5.5: Radioisotopes initial and saturated values and time to reach it, simulating 100 000 000 years with a time span of production of 10 000 years. Where saturation is still not reached the saturation time is defined as >100 000 000 and the saturation value is actually the population of isotopes observable after that time.

Mineral	**Isotope**	**Part. energy**	$\mathbf{N}_0$	$\mathbf{N}_{sat}$	**Time [y]**
Halite	^{10}Be	$\mu+$ at 100 GeV	2	433.8091	31 400 000
	^{10}Be	n at 0.1 GeV	165	3.5789e4	40 950 000
	^{10}Be	n at 1 GeV	754	1.6355e5	44 240 000
	^{40}K	n at 1 GeV	2	1.9470e4	>100 000 000
Morenosite	^{10}Be	$\mu+$ at 100 GeV	3	650.7137	32 280 000
	^{10}Be	n at 0.1 GeV	225	4.8804e4	41 620 000
	^{10}Be	n at 1 GeV	617	1.3383e5	43 810 000
	^{40}K	n at 0.1 GeV	1	9.7350e3	>100 000 000
	^{40}K	n at 1 GeV	147	1.4311e6	>100 000 000
Basalt	^{10}Be	$\mu+$ at 50 TeV	10	2.1690e3	34 890 000
	^{10}Be	$\mu+$ at 100 TeV	3	650.7137	32 280 000
	^{40}K	$\mu+$ at 50 TeV	4	3.8940e4	>100 000 000
	^{40}K	$\mu+$ at 100 TeV	1	9.7350e3	>100 000 000

Conclusions

The work in this elaborate focuses on the passage of two energetic particles, namely a muon and a neutron, in several conditions and materials.
The goal is to study cosmic rays through the analysis of soil samples. This approach is usually called paleodetector.
The results presented in chapter 5 demonstrate that the above-mentioned subatomic particles are effectively able to interact with the encountered materials. Indeed, several isotopes have been found even in the more realistic case arranged with a layer of seawater.
On top of that, also radioactive isotopes have been discovered. Truthfully, this has been an unexpected breakthrough since the elements with a long enough half-life are fairly heavy. Whereas, among the isotopes reported in Table 2.3, two have been observed, namely ^{10}Be and ^{40}K.
Nonetheless, the propagation in time of the just mentioned radioisotopes shows that saturation is not always reached. This may entail that even lighter radioactive elements can be found. Future analysis should investigate elements with a shorter half-life to properly understand whether it is possible or not to find them. Furthermore, different time intervals should be analysed. Indeed, in this work, the radioisotopes have been propagated only over two periods of time and with three different production spans.
To compute the actual population of the isotopes, the fluxes of the secondaries should be considered. This is not done here since the fluxes used in this project are not defined specifically for a high energy cosmic ray's passage. By this is meant that the particles registered within that fluxes are produced by different sources at different energies. Consequently, to evaluate the radio-elements' population

and refine the just obtained models of the isotopes, the muon and the neutron fluxes should be filtered to have only the values concerning the high energy range. However, if the hypothesis stated in the previous chapter is confirmed, the generic fluxes can be used to analyse the radio-isotopes population at saturation without committing significant errors. Indeed, it has been observed that the latter condition is reached almost at the same time in each sample independently from the interval time considered between the passages.

Another fact that should be pointed out is the environment models used. In particular, the oceanic crust has been modelled as a block of basalt. Even though this may not be a too crude approximation, future developments should work to make it more realistic.

Finally, also the simulation should be refined. The complete overview of the cases can be found in Section 4.3. In the first one, the muon enters the environment always from the same location. In future, the particles should enter the detector from a random position within a user defined area. Moreover, the momentum direction has been fixed for every case study. In the advancement of this project, also this parameter should be randomly defined by the simulator.

Nonetheless, the outcomes obtained in this work are optimistic. Indeed, the discovery of both isotopes and radioactive isotopes entails that using soil samples as paleodetectors can be a successful strategy to investigate the passage of cosmic rays.

Truthfully, paleodetectors seem to be the only possibility to search and study past passage events such as the ones that are sought in the GIPETO project. The outcomes of the simulations carried out in this work prove that secondary particles' traces can also be found nowadays. The identification of these traces would demonstrate the past existence of at least one magnetar in our Galaxy.

Bibliography

[1] S. Agostinelli, J. Allison, K. Amako, J. Apostolakis, H. Araujo, P. Arce, M. Asai, D. Axen, S. Banerjee, G. Barrand, F. Behner, L. Bellagamba, J. Boudreau, L. Broglia, A. Brunengo, H. Burkhardt, S. Chauvie, J. Chuma, R. Chytracek, G. Cooperman, G. Cosmo, P. Degtyarenko, A. Dell'Acqua, G. Depaola, D. Dietrich, R. Enami, A. Feliciello, C. Ferguson, H. Fesefeldt, G. Folger, F. Foppiano, A. Forti, S. Garelli, S. Giani, R. Giannitrapani, D. Gibin, J. Gómez Cadenas, I. González, G. Gracia Abril, G. Greeniaus, W. Greiner, V. Grichine, A. Grossheim, S. Guatelli, P. Gumplinger, R. Hamatsu, K. Hashimoto, H. Hasui, A. Heikkinen, A. Howard, V. Ivanchenko, A. Johnson, F. Jones, J. Kallenbach, N. Kanaya, M. Kawabata, Y. Kawabata, M. Kawaguti, S. Kelner, P. Kent, A. Kimura, T. Kodama, R. Kokoulin, M. Kossov, H. Kurashige, E. Lamanna, T. Lampén, V. Lara, V. Lefebure, F. Lei, M. Liendl, W. Lockman, F. Longo, S. Magni, M. Maire, E. Medernach, K. Minamimoto, P. Mora de Freitas, Y. Morita, K. Murakami, M. Nagamatu, R. Nartallo, P. Nieminen, T. Nishimura, K. Ohtsubo, M. Okamura, S. O'Neale, Y. Oohata, K. Paech, J. Perl, A. Pfeiffer, M. Pia, F. Ranjard, A. Rybin, S. Sadilov, E. Di Salvo, G. Santin, T. Sasaki, N. Savvas, Y. Sawada, S. Scherer, S. Sei, V. Sirotenko, D. Smith, N. Starkov, H. Stoecker, J. Sulkimo, M. Takahata, S. Tanaka, E. Tcherniaev, E. Safai Tehrani, M. Tropeano, P. Truscott, H. Uno, L. Urban, P. Urban, M. Verderi, A. Walkden, W. Wander, H. Weber, J. Wellisch, T. Wenaus, D. Williams, D. Wright, T. Yamada, H. Yoshida, and D. Zschiesche, "Geant4—a simulation toolkit," *Nuclear Instruments and Methods in Physics Research Section A: Accelerators, Spectrometers, Detectors and*

Associated Equipment, vol. 506, no. 3, pp. 250–303, 2003, ISSN: 0168-9002. DOI: https://doi.org/10.1016/S0168-9002(03)01368-8. [Online]. Available: https://www.sciencedirect.com/science/article/pii/S0168900203013688.

[2] M. G. Best, *Igneous and Metamorphic Petrology, 2nd Edition*. Wiley-Blackwell, Dec. 2002, pp. 16–50, 316–347, 404–446, ISBN: 978-1-405-10588-0.

[3] W. Bietenholz, *The most powerful particles in the universe: A cosmic smash*, 2013. arXiv: 1305.1346 [physics.hist-ph].

[4] R. M. Bozza, "Una discussione qualitativa dei difetti topologici in cosmologia," Bachelor thesis, Università degli studi di Napoli "Federico II", 2018.

[5] Britannica, The Editors of Encyclopaedia, "Spallation," *Encyclopedia Britannica*, 1998. [Online]. Available: https://www.britannica.com/science/spallation.

[6] ——, "Felsic and mafic rocks," *Encyclopaedia Britannica*, 2006. [Online]. Available: https://www.britannica.com/science/felsic-rock.

[7] ——, "Basalt," *Encyclopaedia Britannica*, 2020. [Online]. Available: https://www.britannica.com/science/basalt.

[8] CERN. (). "Supersymmetry," [Online]. Available: https://home.cern/science/physics/supersymmetry.

[9] G. Consolati, "Lecture notes in space physics," Unpublished, 2020.

[10] R. A. Dunlap, *Particle Physics*, ser. 2053-2571. Morgan & Claypool Publishers, 2018, ISBN: 978-1-64327-362-4. DOI: 10.1088/2053-2571/aae6d3. [Online]. Available: http://dx.doi.org/10.1088/2053-2571/aae6d3.

[11] R. Engel, A. Ferrari, M. Roth, M. Schimassek, D. Schmidt, and D. Vebeič, "Neutron production in extensive air showers," in *Proceedings of 37th International Cosmic Ray Conference (ICRC 2021)*, Online – Berlin, Germany, 2021, pp. 2–6.

[12] R. L. Fleisher, P. B. Price, and R. M. Walker, "Solid-state track detectors: Applications to nuclear science and geophysics," *Annual Reviews*, vol. 15, no. 1, pp. 1–28, 1965.

[13] T. K. Gaisser, R. Engel, and E. Resconi, *Cosmic Rays and Particle Physics*, 2nd ed. Cambridge University Press, 2016. DOI: 10.1017/CBO9781139192194.

[14] GEANT4 collaboration, *Book For Application Developers*, 10.7. CERN Accelerating Science, 2020.

[15] G. Glossary. (). "Object-oriented technology," [Online]. Available: https://www.gartner.com/en/information-technology/glossary/oot-object-oriented-technology.

[16] M. Gordon, P. Goldhagen, K. Rodbell, T. Zabel, H. Tang, J. Clem, and P. Bailey, "Measurement of the flux and energy spectrum of cosmic-ray induced neutrons on the ground," *IEEE Transactions on Nuclear Science*, vol. 51, no. 6, pp. 3427–3434, 2004. DOI: 10.1109/TNS.2004.839134.

[17] C. Grupen, "Basic nuclear physics," in *Introduction to Radiation Protection*, ser. Graduate Texts in Physics. Springer, Berlin, Heidelberg, 2010, pp. 19–30. DOI: https://doi.org/10.1007/978-3-642-02586-0.

[18] K. A. Olive et al. (Particle Data Group), "Leptons," *Chin. Phys.*, vol. C38, 2014. [Online]. Available: http://pdg.lbl.gov.

[19] K. Bernlöhr. (). "Shower detection," [Online]. Available: https://www.mpi-hd.mpg.de/hfm/CosmicRay/ShowerDetection.html.

[20] P. P. Kronberg, "Intergalactic cosmic rays, gamma rays, and magnetic fields," in *Cosmic Magnetic Fields*, ser. Cambridge Astrophysics. Cambridge University Press, 2016, pp. 210–234. DOI: 10.1017/CBO9780511977657.012.

[21] Kudo, Albert M. and Jahns, Richard H., "Igneous rock," *Encyclopaedia Britannica*, 2021. [Online]. Available: https://www.britannica.com/science/igneous-rock.

[22] Matlab. (). "Fit," [Online]. Available: https://www.mathworks.com/help/curvefit/fit.html.

[23] ——, (). "Interp1," [Online]. Available: https://it.mathworks.com/help/matlab/ref/interp1.html#btwp6lt-1-method.

[24] R. Maurer, M. Fraeman, M. Martin, and D. Roth, "Harsh environments: Space radiation environment, effects, and mitigation," *Johns Hopkins APL Technical Digest*, vol. 28, pp. 18–20, Jan. 2008.

[25] S. Mereghetti, J. A. Pons, and A. Melatos, "Magnetars: Properties, origin and evolution," *Space Science Reviews*, vol. 191, no. 1-4, pp. 315–338, Mar. 2015, ISSN: 1572-9672. DOI: 10.1007/s11214-015-0146-y. [Online]. Available: http://dx.doi.org/10.1007/s11214-015-0146-y.

[26] Mindat.org. (). "Halite," [Online]. Available: https://www.mindat.org/min-1804.html.

[27] Mineral Website. (). "Morenosite mineral data," [Online]. Available: http://webmineral.com/data/Morenosite.shtml#.YTeDFo4zZPZ.

[28] National Geographic. (). "Atmosphere," [Online]. Available: https://www.nationalgeographic.org/encyclopedia/atmosphere/.

[29] National Ocean Service. (). "How deep is the ocean?" [Online]. Available: https://oceanservice.noaa.gov/facts/oceandepth.html.

[30] K. A. Olive, "Review of particle physics," *Chinese Physics C*, vol. 38, p. 09 001, Aug. 2014. DOI: 10.1088/1674-1137/38/9/090001.

[31] M. Paz Arribas, "Estimation of trigger rates, data rates and data volumes for cta and observations of snr rx j0852.0-4622 with h.e.s.s.," Ph.D. dissertation, Humboldt-Universität zu Berlin, Jul. 2017. DOI: 10.18452/18056.

[32] M. Perfit, "Earth's oceanic crust," *Encyclopedia of Earth Sciences Series*, pp. 2–9, Jan. 2016. DOI: 10.1007/978-3-319-39193-9_266-1.

[33] S. V. Polyakov, "Chapter 3 - photomultiplier tubes," in *Single-Photon Generation and Detection*, ser. Experimental Methods in the Physical Sciences, A. Migdall, S. V. Polyakov, J. Fan, and J. C. Bienfang, Eds., vol. 45, Academic Press, 2013, pp. 69–82. DOI: https://doi.org/10.1016/B978-0-12-387695-9.00003-2. [Online]. Available: https://www.sciencedirect.com/science/article/pii/B9780123876959000032.

[34] P. B. Price and R. M. Walker, "Chemical etching of charged-particle tracks in solids," *Journal of Applied Physics*, vol. 33, no. 12, pp. 3407–3412, 1962. DOI: 10.1063/1.1702421. eprint: https://doi.org/10.1063/1.1702421. [Online]. Available: https://doi.org/10.1063/1.1702421.

[35] Science Learning Hub. (). "Ocean salinity," [Online]. Available: https://www.sciencelearn.org.nz/resources/686-ocean-salinity.

[36] Z. Szadkowski, "Introductory chapter: Ultrahigh-energy cosmic rays," in *Cosmic Rays*, Z. Szadkowski, Ed., Rijeka: IntechOpen, 2018, ch. 1. DOI: 10.5772/intechopen.79535. [Online]. Available: https://doi.org/10.5772/intechopen.79535.

[37] A. Veutro, "Modelizzazione della propagazione di raggi cosmici di altissima energia prodotti da magnetar galattiche," Bachelor thesis, Università degli studi di Milano, 2020.